INVESTIGATING BIOLOGICAL SAMPLES WITH ATOMIC FORCE MICROSCOPE: FROM LIVING CELLS TO MOLECULAR LEVEL

PhD Thesis

Zoltán Bálint

Supervisor: Dr. György Váró

Institute of Biophysics
Biological Research Centre
Hungarian Academy of Sciences
Szeged, Hungary

2006

Contents

Acknowledgements

This thesis is the result of work and study in the Institute of Biophysics, Biological Research Center of the Hungarian Academy of Sciences. During my stay in Szeged I was accompanied and supported by many people to whom I wish to acknowledge now.

First of all, I would like to express my deepest gratitude to my supervisor, György Váró, who introduced me to the field of biophysics. During my whole PhD student period I was impressed and got inspired by his way of thinking about science and life. His careful guidance developed my experimental skills and our everyday debates about the projects broadened my knowledge and made my work and life easy.

I wish to acknowledge my colleague, Zsolt Szegletes for the time we spent together during installing, developing the AFM system, learning the technique and for his useful advices during my work and studies.

I am grateful to Imola Wilhelm and István A. Krizbai for the cell cultures and the neurobiological background. I express my appreciation to Márta Dorogi, László Nagy and Klára Hernádi for providing me the protein and nanotube samples and for the valuable discussions on their function and interaction. I wish to acknowledge Ilona Hollósiné Laczkó and Sándor Bottka for involving me in the peptide - oligonucleotide interaction studies.

I would like to thank to Pál Ormos, the director of the Institute of Biophysics, and all the members of the Institute for creating the stimulating atmosphere and giving interesting feedbacks and valuable discussions.

I particularly appreciate the German representatives of the Asylum Research Company, especially Stefan Vinzelberg, for the continuous assistance and technical help.

Special thanks go to my parents and my sister for their support and love, and to all of my friends who were with me during this period. Last, but always first, my greatest gratitude goes to my wife for her love, understanding and for being a constant source of support for me.

List of Abbreviations

AC mode	-	**alternative contact mode**
AFM	-	**atomic force microscope**
ATR-FTIR	-	**attenuated total reflection - Fourier-transformed infrared spectroscopy**
BBB	-	**blood brain barrier**
CEC	-	**cerebral endothelial cell**
CD	-	**circular dichroism**
DMEM/F12	-	**Dulbecco's Modified Eagles Medium with F12 salt**
EM	-	**electron microscope**
EPR	-	**electron paramagnetic resonance**
ESI-MS	-	**electrospray ionization mass spectrometry**
FBS	-	**fetal bovine serum**
GFP	-	**green fluorescent protein**
hCMEC/D3	-	**human cerebral microvascular endothelial cell**
HiPco	-	**high-pressure carbon monoxide process**
HUVEC	-	**human umbilical vein endothelial cell**
MDCK cell	-	**Madine-Darby canine kidney cell**
MFP-3D	-	**Molecular Force Probe 3D**
ODN	-	**oligonucleotide**
Pal-SV peptide	-	**palmitoylated simian virus peptide**
PBS	-	**phosphate-buffered saline**
RC	-	**photosynthetic reaction center**
RP-HPLC	-	**reverse-phase high pressure liquid chromatography**
SPM	-	**scanning probe microscope**
STM	-	**scanning tunneling microscope**
SV 40	-	**simian virus 40**
SWNT	-	**single-walled carbon nanotube**
TEM	-	**transmission electron microscope**

Publication List

Papers related to the thesis:

I. Dorogi M., **Z. Bálint**, C. Mikó, B. Vileno, M. Milas, K. Hernádi, L. Forró, G. Váró and L. Nagy. 2006. Stabilization effect of single walled carbon nanotubes on the functioning of photosynthetic reaction centers. *Journal of Physical Chemistry B.* 110 (43):21473-21479.

II. Laczkó I., G. Váró, S. Bottka, **Z. Bálint**, E. Illyés, E. Vass, J.-R. Bertrand, C. Malvy and M. Hollósi. 2006. N-Terminal acylation of the SV40 nuclear localization signal peptide enhances its oligonucleotide binding and membrane translocation efficiencies. *Archives of Biochemistry and Biophysics.* 454 (2):146-154.

III. **Bálint Z.**, I.A. Krizbai, I. Wilhelm, A.E. Farkas, Á. Párducz, Z. Szegletes and G. Váró. 2006. Changes induced by hyperosmotic mannitol in cerebral endothelial cells: an atomic force microscopic study. *European Biophysical Journal.* In press.

Other papers:

IV. Dioumaev A.K., J.M. Wang, **Z. Bálint**, G. Váró, and J.K. Lanyi. 2003. Proton transport by proteorhodopsin requires that the retinal Schiff base counterion Asp-97 be anionic. *Biochemistry-US* 42:6582-6587.

V. **Bálint Z.,** M. Lakatos, C. Ganea, J.K. Lanyi, and G. Váró. 2004. The nitrate transporting photochemical reaction cycle of the pharaonis halorhodopsin. *Biophysical Journal* 86:1655-1663.

VI. Magyari K., **Z. Bálint**, V. Simon and G. Váró. 2006. The photochemical reaction cycle of retinal reconstituted bacteriorhodopsin. *Journal of Photochemistry and Photobiology B: Biology* 85(2):140-144.

1. Introduction

1.1. General

In the early 1980's the microscopy was revolutionized by the invention of the scanning tunneling microscope (STM) by Binnig and Rohrer. The STM was the first member of the large family of scanning probe microscopes (SPM), which scans a surface with a sharp probe and senses its structure by measuring the interaction between the probe and the surface. The STM measures the tunneling current between a conductive surface and probe. Binnig and Rohrer's work was recognized with Nobel Prize in Physics in 1986.

Binnig and colleagues developed further this technique and in 1986 they presented the second member of the SPM family – the atomic force microscope (AFM) (Binnig et al., 1986). This instrument records topography based on the monitoring of the probe deflection caused by the surface roughness dominated by van der Waals interaction. Commercial AFM's became available in the early 1990's and were refined during the past years. Nowadays dozens of different types of AFM's are available in the market, with applications in material-, chemical-, physical-, biological sciences, medicine and even in industry.

Conventional microscopes image by collecting the transmitted or reflected light from the sample. Their resolution is diffraction limited and depends on the radiation wavelength. Higher resolution images can be obtained by the electron microscope (EM) using high energy electrons, although this technique has the disadvantage that the samples have to be examined under vacuum.

As the SPM measures changes in the interaction between the probe and sample surface, its resolution depends on the sharpness of the tip, the sample positioning accuracy relative to the probe and the detection of the probe motion. Its resolution goes far beyond of optical microscope's. The main advantage of this technique is that it can be easily used to image with high resolution in gaseous or liquid environments. This made it suitable for biological applications, because it is able to visualize biological objects and biological processes under physiological conditions. They offer the resolution of the electron microscope under the experimental conditions of conventional light microscopes and even more.

1.2. The atomic force microscope

The atomic force microscope uses a very sharp needle at the end of a cantilever, which comes into contact with the sample surface and scans by moving on it. The instrument records surface topography with high resolution. A laser beam reflected from the upper part of the cantilever, collected by a four segment photodiode, is used to monitor its movement (Fig. 1.). There is a feedback loop which connects the photodiode signal with the piezoelectric scanner. When the tip moves on the surface, the laser spot on the photodiode will move also and the piezo will lift the cantilever to recover the position of the spot. By recording the vertical piezo movement the surface topography can be constructed.

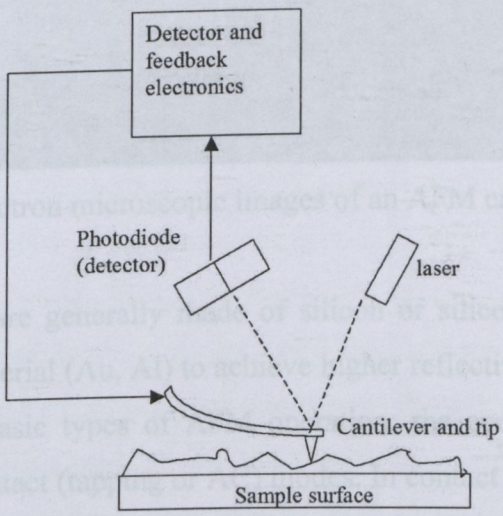

Fig. 1. The block diagram of an atomic force microscope.

The scanning mechanism is realized by piezoelectric transducers. If a potential difference is applied on the piezoelectric material (piezo) it will expand. This motion is reproducible and so sensitive, that the piezo can be made to move with atomic resolution accuracy. There are different technical realizations. Conventional types of AFMs use a piezoelectric tube scanner on which the sample is mounted and this tube moves the sample relative to the tip in all three orthogonal directions. In the case of the Molecular Force Probe (MFP-3D) system the sample stage contains two distinct linear piezos which are moving the

sample in x and y directions, whereas the vertical movement is realized by a third piezo, mounted on the cantilever holder. This new concept offers a more stable and more precise movement of the sample relative to the tip.

The main part of the system is the cantilever. To achieve such high resolution special, very sharp tips are needed. Usually an AFM cantilever has several hundreds of microns length, and at the very end of it there is a few micron high, pyramidal shape tip, with an apex of few nanometers (Fig. 2.).

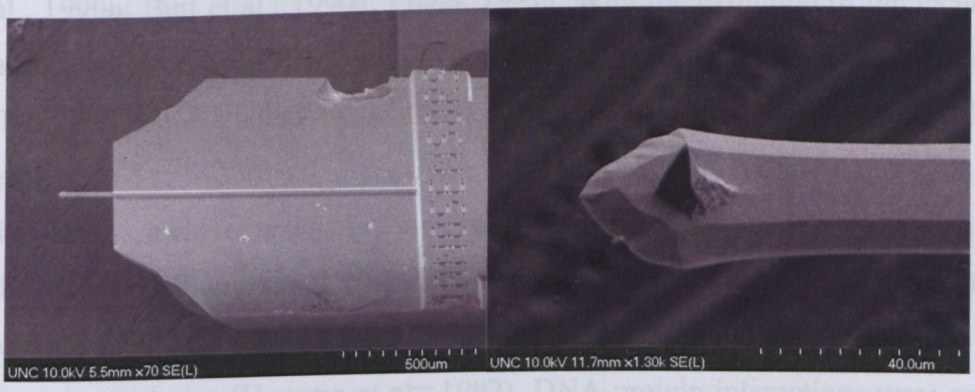

Fig. 2. Electron microscopic images of an AFM cantilever and tip.

The cantilevers are generally made of silicon or silicon nitrate and they are coated with some reflective material (Au, Al) to achieve higher reflectivity of the laser beam.

There are two basic types of AFM operation: the constant force (contact) and the resonant intermittent contact (tapping or AC) modes. In contact mode the cantilever's bending (deflection) is kept constant at a certain, predefined set-point and for any deviation from this value, caused by the surface roughness, the vertical piezo reacts. By this predefined set-point the force exerted by the cantilever on the sample can be kept constant and determined by knowing the parameters of the cantilever (Hoh and Schoenenberger, 1994). Error signal (deflection) images are captured recording any deviation from the set-point deflection value of the cantilever during scanning.

In AC mode the cantilever is oscillated usually at or near its resonance frequency with a few nanometer amplitude and its damping caused by the sample surface is kept constant. Any surface roughness causes variations on the amplitude value which is used to drive the feedback. Any deviations from the set-point amplitude value of the oscillating cantilever are

recorded and the error signal image constructed. The AC mode operation was introduced to minimize tip-sample interaction time during scanning and it is suitable for investigate soft biological materials by reducing the possible sample damages caused by the relative hard tip.

1.3. Studying biological objects at high resolution

Although the AFM was developed for nanometer scale investigation of solid sample's topography (Binnig et al., 1986) the first biological applications were reported very soon (Butt et al., 1990b; Butt et al., 1990a; Engel, 1991). With the evolution of the technique and the appearance of biology-specialized AFMs the possibilities expanded. Since than different biological objects were studied from whole cells and bacteria down to single DNA and protein level.

The first and extensively investigated biological object was the DNA. The conformation, size and shape of it were studied (Hansma et al., 1992; Hansma et al., 1993; Hansma and Hoh, 1994). The persistence length was calculated and the α-helical structure was imaged also (Hansma et al., 1992). DNA-protein interactions were extensively studied (Hansma et al., 1994; Bustamante and Rivetti, 1996). Since than different forms and types of DNA were observed, including fragments of DNA, the oligonucleotides (ODN) (Cherny et al., 1998; Costa et al., 2004; Mourougou-Candoni et al., 2003). ODNs and their complexes with poly(ethyleneimine) were monitored (Brus et al., 2004). Immobilized ODNs on protein surface were visualized (Kim et al., 2004). This technique opened the possibility to study protein - DNA interactions *in situ* (Bennink et al., 2003).

Beside DNA, Müller and coworkers managed to visualize single membrane proteins with unprecedented resolution (Muller et al., 1995; Muller et al., 1997; Muller et al., 1999). Single titin molecules were imaged and their physical properties were investigated (Kellermayer et al., 2003). The native membranes of different photosynthetic bacteria were imaged (Scheuring et al., 2004; Scheuring et al., 2005). The light harvesting complexes of a native photosynthetic apparatus were visualized with single molecular resolution (Goncalves et al., 2005). With an atomic force sensing system the light induced protein dynamics of bacteriorhodopsin and photosynthetic reaction centers were detected with microsecond time resolution (Rousso et al., 1997).

1.4. Atomic force microscopy on cells

In the same time whole cell studies evolved as well. A broad range of cell types have been studied including endothelial cells (Braet et al., 1997; Oberleithner et al., 2003; Pesen and Hoh, 2005a), fibroblasts (Rotsch and Radmacher, 2000), epithelial cells (Sharma et al., 2005; Jimenez-Garcia and Fragoso-Soriano, 2000) and osteoblasts (Domke et al., 2000).

Beside topographical images and morphological changes of living cells, the AFM provides information about material properties. The elastic modulus of different cells have been studied, such as platelets (Radmacher et al., 1996), epithelial cells (Hoh and Schoenenberger, 1994), cardiocytes (Hofmann et al., 1997), fibroblasts (Wu et al., 1998). It was also possible to monitor time dependent variations in mechanical properties of epithelial cells (Hassan et al., 1998) and other cellular processes (Kuznetsov et al., 1997). The use of AFM added a new tool to study the effect of different drugs and extracellular stimuli on living cells (Oberleithner et al., 2003). Furthermore, different aspects of cellular function such as cell growth on different surfaces (Chung et al., 2003; Domke et al., 2000), Ca^{2+} depletion induced volume changes (Quist et al., 2000) or drug administration effects (Rotsch and Radmacher, 2000) have been studied as well. The AFM proved to be a unique imaging tool of cytoskeletal organization and visualization of its changes in living cells (Le Grimellec et al., 1998; Mahaffy et al., 2004; Berdyyeva et al., 2005; Pesen and Hoh, 2005a; Pesen and Hoh, 2005b).

The local force measurements on the surface of cells have revealed the elastic properties of different cellular regions and structures (Vinckier and Semenza, 1998; Sato et al., 2004; Wojcikiewicz et al., 2004; Sharma et al., 2005; Wu et al., 1998).

One of the most intensively studied cell type with the AFM is the endothelial cell. Considerable parts of the studies were performed on human umbilical vein endothelial cells (HUVECs). Beside their mechanical characteristics (Mathur et al., 2001; Sato et al., 2004), single molecule binding events (Pfister et al., 2005), cell-cell interactions (Zhang et al., 2003), growth rate (Chung et al., 2003) and the effect of drugs (Oberleithner et al., 2003) have been studied. The cytoskeletal structure of pulmonary microvascular endothelial cells were revealed (Pesen and Hoh, 2005a; Pesen and Hoh, 2005b). Cultured rat hepatic sinusoidal

endothelial cells were studied after drying them (Braet et al., 1997). Little is known about cerebral endothelial cells (CECs).

1.5. The blood brain barrier and the endothelial cells

Our special interest was the influence of different external conditions upon living cells. As subject of this study the cerebral endothelial cells (CECs) were chosen. They are important components of the blood brain barrier (BBB), which is the interface between the peripheral circulation and the central nervous system. The tight junctions between the endothelial cells restrict diffusion of water-soluble substances from blood to brain. Disruption of the tight junctions can lead to improper BBB function (Hawkins and Davis, 2005).

In certain cases the BBB can be an impediment for the chemical treatment of diseases of the central nervous system. Attempts have been made to overcome this by linking the active compound to a carrier (Pardridge, 2002). An alternative possibility is the reversible opening of the BBB. High concentration of mannitol was successfully used for this purpose both experimentally and clinically, although the mechanism of osmotic disruption is not well understood (Rappoport et al., 2000; Neuwelt et al., 1991; Kroll and Neuwelt, 1998; Doolitle et al., 2000). It has been shown that mannitol induces reversible phosphorylation of β-catenin, a protein of the intercellular junctional complex in CECs (Farkas et al., 2005), which might contribute to the BBB opening. However further information is needed about the effect of mannitol on CECs.

Extracellular calcium removal and readdition (calcium switch) is a frequently used method for studying tight junction biogenesis. However, details regarding the mechanism, time scale and morphological changes are still missing. There are some recent data about the endocytosis of junctional proteins in epithelial cells (Ivanov et al., 2004), however very few is known about the changes induced by calcium switch in CECs.

1.6. The aim of the work

The objective was the micro- and nanometer scale characterization of different biological samples such as surface-dried peptides and oligonucleotides, photosynthetic reaction centers and the investigation of living cell's surface and their responses to different extracellular stimuli.

For this purpose the complexes formed by Pal-SV modified nuclear localization signal peptide and 18 mer oligonucleotide were studied at different concentrations, air-dried onto mica surface and imaged in air. If they form stable complex, the ODN can be delivered onto the cell nucleus from the extracellular space.

Another subject of the study was the bacterial photosynthetic reaction center (RC). The interaction of single walled carbon nanotubes (SWNTs) and RCs air-dried onto mica surface was studied to strengthen the idea that they form stable complexes.

To get an insight into different cellular processes, the surface and mechanical properties of living cerebral endothelial cells (CECs) have been studied. After imaging the cells under normal conditions in medium, the effect of different extracellular chemical factors, such as mannitol and low level of calcium, were studied.

To successfully monitor the cellular changes, first the imaging parameters and conditions were stabilized by recording topographies of some cell types (epithelial, fibroblasts, endothelial) in different operating modes. The hyperosmotic effect of mannitol was demonstrated by comparing subsequent images of the same CECs. By measuring the cell elasticity, information was gathered from changes occurring deep inside the cells.

Details regarding the mechanism and morphological changes of CECs induced by the calcium switch were missing. With the AFM it was possible to monitor the surface and volume changes of living CECs in the process of their recovery after calcium depletion.

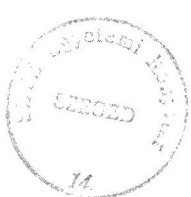

2. Materials and Methods

2.1. Sample preparation

In order to investigate the surface of the samples they had to be immobilized on the surface, else they would have been pushed away by the AFM tip. The easiest way to immobilize the biological samples is to dry them onto flat surface.

As a support for studying dried biological samples, mica was used. The muscovite mica is a yellowish, light-colored, transparent to translucent silicate (subclass: phyllosilicates) mineral with the following chemistry: $K_2Al_4Si_6Al_2O_{20}(OH,F)_4$, potassium aluminum silicate hydroxide fluoride. It is a hard, layered, crystalline material that fractures along weak atomic planes ("cleavage" planes), thus easily producing atomically flat surfaces, having a regular lattice structure, excellent for high-resolution AFM studies. Muscovite has a layered structure of aluminum silicate sheets weakly bonded together by layers of potassium ions. The potassium ions occupy large holes between 12 oxygen atoms, 6 from the layer above and 6 from the layer below; the resulting K-O ionic bonds are rather weak and can be easily broken. The cleavage sheets are fairly flexible and elastic, hydrophilic, and negatively charged in water. The 15 x 15 mm^2 mica sheets (SPI Supplies Division, West Chester, PA, USA) were freshly cleaved before each measurement.

2.2. Peptide and oligonucleotide synthesis

The modified SV40 (^{126}Pro-Lys-Ser-Lys-Arg-Lys-Val-Ser^{133}) nuclear localization signal peptide sequence, $SV_{126\text{-}133}(Ser^{128})$ was synthesized with free N-terminal, and also bearing a palmitoyl group at the N-terminus (Pal-SV). Peptides were prepared by manual solid phase methodology, using Boc/Bzl strategy (Stewart and Young, 1984) and 4-methyl benzhydrylamine resin (0.7 mM/g). All amino acids were coupled as Boc-derivatives. Octanoic acid and palmitic acid were coupled as the Boc amino acids. The crude products were analyzed, purified and checked for the homogeneity by reverse phase high pressure liquid chromatography (HPLC). The identification of the peptides was achieved by

electrospray ionization mass spectrometry (ESI-MS) using a Bruker Daltonics Esquire 3000 Plus (Bremen, Germany) mass spectrometer.

The GFP-targeted oligonucleotide (18 mer) with the following sequence: 5' GAGCTGCACGCTGCCGTC 3', was synthesized with an Expedite 8909 synthesizer (Applied Biosystems, USA), using solid-supported standard β-cyanoethyl phosphoramidite chemistry at a nominal scale of 1 μM. Purification was performed by HPLC on a Kromasil 100-C18 250 x 10 mm ID column, using a MeCN-0.1 M triethylammonium acetate (pH 7.0) mixture as eluent. This results in the triethylammonium salt of ODN.

The peptide and ODN samples were synthesized and provided by our coworkers: Sándor Bottka and Ilona Hollósiné Laczkó.

Fifty microliters of an aqueous solution of Pal-SV peptide, ODN or their mixture at molar ratio (r_M) values of 1 and 20 was dropped onto a freshly cleaved mica surface and dried for 1 h under a continuous flow of high purity air.

2.3. Carbon nanotubes and bacterial photosynthetic reaction centers

Commercially available single walled carbon nanotubes (SWNTs), produced by a high-pressure carbon monoxide process (HiPco), have been purchased from Carbon Nanotechnologies Incorporated Company and were purified by wet oxidation technique. Raw HiPco SWNTs (100 mg) were oxidized in a mixture of 60 mL of 30% H_2O_2 and 110 mL of 22% HCl (Hernadi et al., 2001). The suspension was then refluxed under continuous magnetic stirring at 70 °C for 9 h and it was cooled to room temperature. The SWNTs were filtered and washed with distilled water at pH 7. Finally, SWNTs were dried at 120 °C for 30 min. The yield of purified SWNTs was 90%, determined by transmission electron microscopy (TEM). From the TEM data it resulted that the average diameter of the tubes was 1.5 nm.

Rhodobacter sphaeroides R-26 cells were grown photoheterotrophically. RCs were prepared by LDAO (*N,N*-dimethyldodecylamine-*N*-oxide, Fluka) solubilization and purified by ammonium sulfate precipitation, followed by DEAE Sephacel (Sigma) anion-exchange chromatography (Tandori et al., 1995). After preparation, the RC QB site was reconstituted by the addition of ubiquinone-10 (UQ-10) and concentrated by centrifuge filter (Whatman VectaSpin 3, 10 kDa exclusion) to 80-100 μM.

To bind RCs to SWNTs 500 μL of LDAO solubilized RCs were incubated with the suspension of SWNT and subjected to intensive dialysis against 750 cm^3 of distilled water for 3 days. The distilled water was changed and the suspension was sonicated in a water bath (10 s continuously, ELMA Transsonic 310) every 12 h. The RC concentration was kept as high as possible, routinely 80-100 μM. The mass-to-mass ratio was routinely 10 ± 3 mg RC/mg SWNT. After the dialysis, the sample was sedimented by ultracentrifuge (100,000 x g, 20 min, SORVALL ULTRA Pro, A-1256 rotor), and the precipitate was suspended in distilled water by sonication for 10-20 s. The supernatant was checked for the unbound RCs, and the resuspended precipitate was subjected to second ultracentrifugation. Finally, the precipitate was resuspended in about 500 μL of distilled water.

The protein and carbon nanotube samples were provided by our coworkers: Márta Dorogi, László Nagy and Klára Hernádi.

For the AFM measurements 50 μl of sample have been dried for 1 h under a continuous flow of high purity air onto freshly cleaved mica surface.

2.4. Cell cultures

GP8 rat brain endothelial cells (Greenwood et al., 1996) were cultured in 3.5 cm diameter Petri dishes (Falcon) coated with rat tail collagen in DMEM/F12 (Dulbecco's Modified Eagles Medium with F12 salt, Sigma, a medium with physiological concentrations of inorganic salts, amino acids, vitamins, D-Glucose (3.15 g/l), HEPES, phenol red) supplemented with 12% PDS (Plasma Derived Serum, First Link, UK) at 37 °C in 5% CO_2. Cells were grown until confluency. In the course of the experiment the medium was exchanged with the same solution, containing 0.55 M mannitol (Sigma).

Madine-Darby canine kidney (MDCK) epithelial cells were cultured in 3.5 cm diameter Petri dishes (Falcon) in DMEM/F12 (Sigma) medium supplemented with 10% fetal bovine serum (FBS, Sigma) at 37 °C in 5% CO_2 containing atmosphere. Cells were grown until confluency. To fix the cells, they were washed with PBS (phosphate-buffered saline), followed by fixation in etanol/acetic acid (95/5) for 10 min at -20 °C. The cells after fixation were washed with PBS.

Immortalized human brain endothelial cells (hCMEC/D3) were routinely grown on rat tail collagen-coated plates in EGM-2 medium (Cambrex) supplemented with 5 % FBS (Sigma). The Ca^{2+} depletion was performed in serum free medium (Sigma, M8167) for 30 - 150 minutes followed by a 30 - 300 minutes recovery in serum free DMEM/F12 medium.

Fibroblast cells (3T3/L1) were grown in high glucose containing DMEM (Dulbecco's Modified Eagles Medium) containing 10 % FBS (Sigma).

The cell cultures were grown by our coworkers: Imola Wilhelm and István A. Krizbai.

The AFM measurements on cells were done by placing the Petri dish with the culture on the sample stage of the instrument and working in cell-specific medium.

2.5. Instrumentation setup, cantilevers and measuring conditions

All the measurements were performed with an Asylum MFP-3D head and Molecular Force Probe controller (Asylum Research, Santa Barbara, CA, USA). The driver program MFP Xop was written in IGOR Pro software (version 5.0.3, Wavemetrics, Lake Oswego, OR, USA). The scheme of the instrument is presented on the Fig. 3.

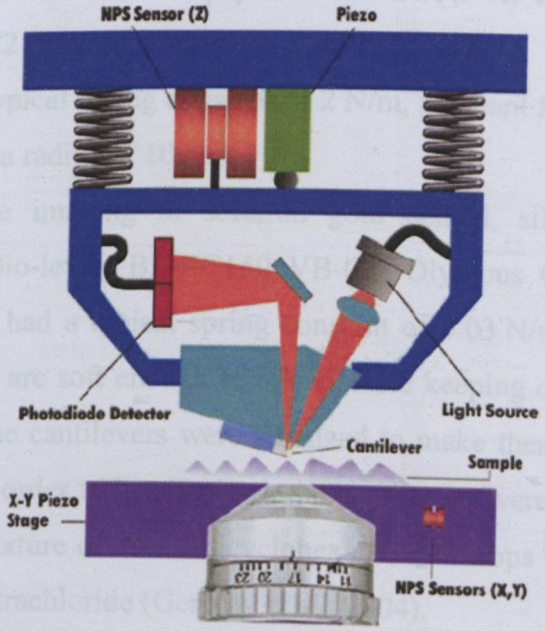

Fig. 3. The scheme of the MFP-3D type atomic force microscope.

The AFM was equipped with a 100 x 100 μm piezo stage and with an 8 μm working distance vertical piezo. The lateral piezos had a 90 μm travel in closed loop, with a sensor noise <0.6 nm. The vertical piezo had a noise <0.06 nm.

The MFP-3D head was mounted on a Zeiss Axiovert 200 invert optical microscope. The AFM is extremely sensitive to external noises. In order to isolate the system the whole setup was placed on a pneumatic vibration isolation table (Supertech, Hungary) and on an active vibration isolation system (MOD1-M, Halcyonics GmbH, Germany). For acoustic isolation a home-made plastic cage was used, which covers the MFP-3D head and sample stage, offering temperature and humidity control as well.

All the cantilevers were calibrated before measurements by the thermal method and by recording a force curve on a hard surface (Hutter and Bechhoefer, 1993). The spring constant of each cantilever was calculated by the software of the instrument.

For AC mode measurement on photosynthetic reaction centers and carbon nanotubes Al coated, silicon rectangular cantilevers (AC160TS-C2 Olympus Optical Co. Ltd., Tokyo, Japan) have been used. These cantilevers had a typical spring constant of 42 N/m, resonant frequency of 300 kHz and a tetrahedral shape tip with a radius of 10 nm.

For AC mode measurement on peptides and ODNs Al coated, silicon rectangular cantilevers (AC240TS-C2 Olympus Optical Co. Ltd., Tokyo, Japan) have been used. These cantilevers had a typical spring constant of 2 N/m, resonant frequency of 70 kHz and a tetrahedral shape tip with a radius of 10 nm.

For contact mode imaging in solution gold coated, silicon nitride, rectangular cantilevers were used (Bio-lever, BL-RC150 VB-C1, Olympus Optical Co. Ltd., Tokyo, Japan). These cantilevers had a typical spring constant of 0.03 N/m and V-shape tip with a radius about 30 nm. They are soft enough to allow stable keeping of the exerted force in the hundreds of pN range. The cantilevers were silanized to make them hydrophobic, hindering the tip-cell interaction. In order to be silanized, the cantilevers were incubated overnight in a closed chamber with a mixture of 10 ml bicyclohexane, 1-4 drops of octadecyltrichlorsilane and 4-8 drops of carbon tetrachloride (Gergely et al., 2004).

For AC mode in liquid the same Bio-lever type cantilevers were used or silicon nitride, rectangular cantilevers with tetrahedral tip (Bio-lever mini, BL-AC40TS-C2,

Olympus Optical Co. Ltd., Tokyo, Japan). These cantilevers had a typical spring constant of 0.09 N/m and a resonant frequency of 110 kHz in air, respectively 25 kHz in water.

2.6. Force measurements

Apart from topography acquisition, the AFM can be used for force measurement as well. In this case the tip is engaged on a certain point on the surface and its deflection is monitored in function of the vertical piezo movement. A scheme of a force curve acquired on a hard surface in air is presented on Fig. 4. During the engagement the deflection of the cantilever will start to increase at the moment when the tip reaches the surface (Fig. 4. red line). On the way back, because of the adhesion forces, it will be stacked to the surface (Fig. 4. blue line).

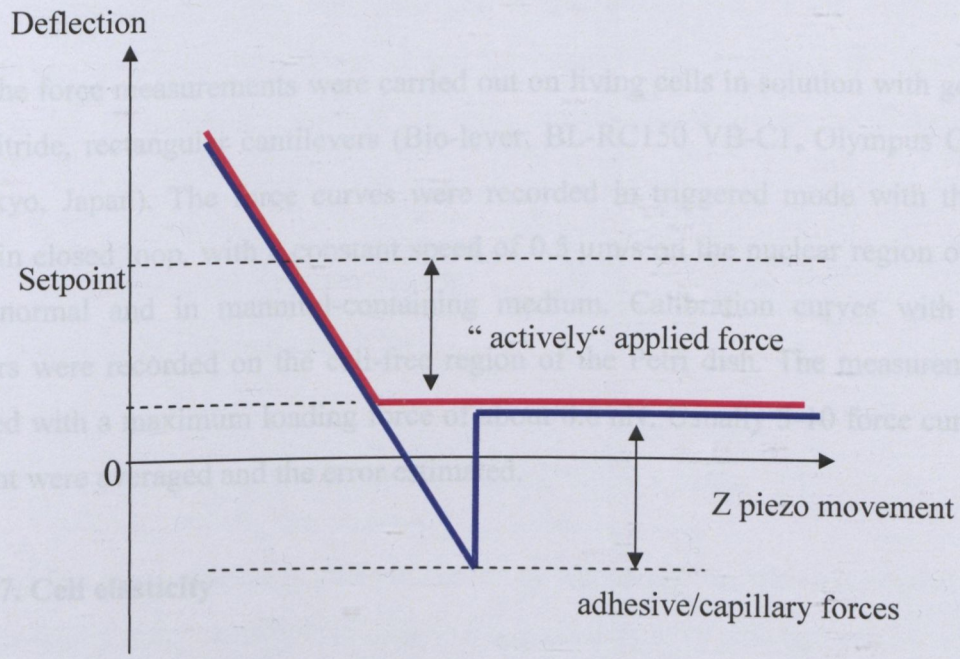

Fig. 4. Scheme of a force curve taken on a hard surface.

In liquid environment on soft samples there is less adhesion and the force curve will be like the one presented on Fig. 5. The x axis of the curve is expressed in terms of working distance of the z piezo. Its absolute value depends on the force measurement parameters.

If the force measurement is realized on soft samples besides the cantilever bending it presses the sample, causing its indentation (Vinckier and Semenza, 1998; Mathur et al., 2001).

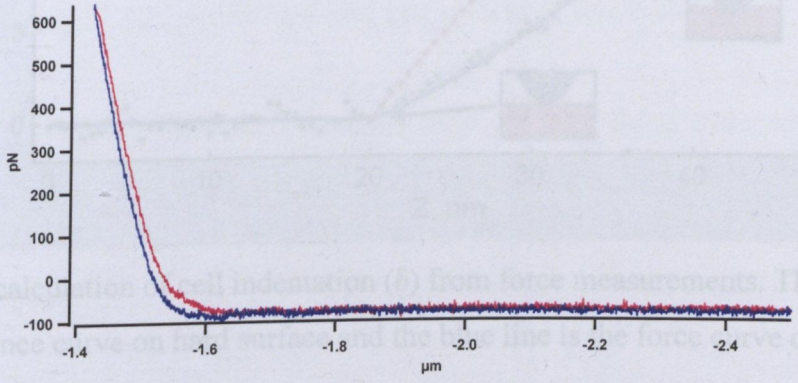

Fig. 5. A typical force curve taken on soft material in liquid. The red curve is the approaching and the blue curve is the retraction of the cantilever.

The force measurements were carried out on living cells in solution with gold coated, silicon nitride, rectangular cantilevers (Bio-lever, BL-RC150 VB-C1, Olympus Optical Co. Ltd., Tokyo, Japan). The force curves were recorded in triggered mode with the Z piezo working in closed loop, with a constant speed of 0.5 µm/s on the nuclear region of the cells, both in normal and in mannitol-containing medium. Calibration curves with the same parameters were recorded on the cell-free region of the Petri dish. The measurements were effectuated with a maximum loading force of about 0.6 nN. Usually 5-10 force curves on the same point were averaged and the error estimated.

2.7. Cell elasticity

To calculate the Young's moduli of the cells only the approaching part of the curves were used to avoid the effect of the tip-cell membrane interaction. By subtracting the reference force curve, measured on a hard surface, from the curves measured on the cells, the indentation can be obtained (Fig. 6.). These curves provide information about the material stiffness (Vinckier and Semenza, 1998).

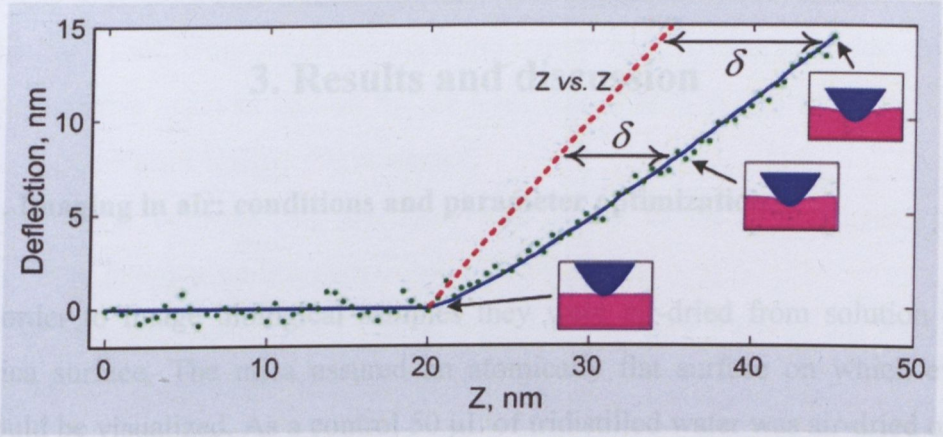

Fig. 6. The calculation of cell indentation (δ) from force measurements. The red line is a reference curve on hard surface and the blue line is the force curve on cells.

To obtain the Young's modulus the theory based on the work of Hertz (Hertz, 1881) and Sneddon (Sneddon, 1965) was used and further developed for the case of the AFM technique (Mathur et al., 2001; Vinckier and Semenza, 1998). The force as a function of the indentation Δz, considering a conical tip with opening angle α can be described by the equation:

$$F(\Delta z) = \frac{2E^*}{\pi(tg(\alpha))}\Delta z^2 \qquad (1)$$

where E^* is the relative Young's modulus:

$$\frac{1}{E^*} = \frac{1-\mu^2_{cantilever}}{E_{cantilever}} + \frac{1-\mu^2_{sample}}{E_{sample}} \qquad (2)$$

Considering that the cantilever is made of silicon or silicon nitride, which is several orders of magnitudes harder than the sample ($E_{sample} << E_{cantilever}$) the above equation can be simplified:

$$\frac{1}{E^*} \approx \frac{1-\mu^2_{sample}}{E_{sample}} \qquad (3).$$

In this case E_{sample} is the Young's modulus and μ_{sample} is the Poisson ratio of the cell (Vinckier and Semenza, 1998).

3. Results and discussion

3.1. Imaging in air: conditions and parameter optimization

In order to image biological samples they were air-dried from solution on freshly cleaved mica surface. The mica assured an atomically flat surface on which even single peptides could be visualized. As a control 50 µL of tridistilled water was air-dried on the mica surface and imaged (Fig. 7.).

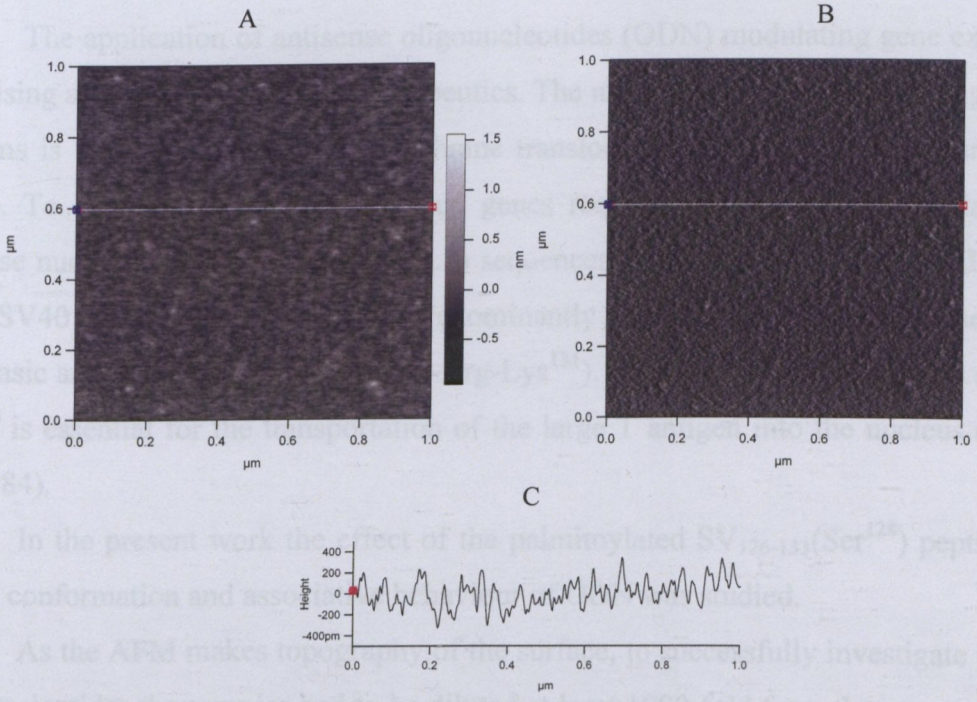

Fig. 7. 1 x 1 μm^2 (A) height image, (B) error signal (amplitude) and (C) the height profile along the line shown on the image of tridistilled water dried on mica surface.

The images were recorded in AC mode with a free amplitude damping of 20%. The integral and proportional gain values (determining the response of the feedback) were set as high as possible, avoiding the oscillation of the feedback loop. The scanning rate was 2 Hz (2 lines/s) resulting in a scanning speed of 4 µm/s for a 1 x 1 μm^2 image.

Usually 512 x 512 scan points were taken, which meant a ~2 nm lateral resolution in the case of a 1 x 1 μm^2 image. Both the trace and retrace images were recorded and compared to eliminate possible artifacts caused by the scan speed and the cantilever shape. For this reason here only the trace images are presented.

The surface roughness of the mica was found to be 0.3 ± 0.1 nm, which was sufficiently flat to image even few nanometer high structures.

Before each experiment with ODNs, peptides, RCs and SWNTs this kind of control was done to assure the reliability of the obtained images.

3.2. Oligonucleotides and peptides

The application of antisense oligonucleotides (ODN) modulating gene expression is a promising approach of medicinal therapeutics. The major limitation of non-viral gene delivery systems is the low efficiency of membrane translocation and targeting (Luo and Saltzman, 2000). To become effective, transfected genes require delivery into the nucleus. For this purpose nuclear localization signal (NLS) sequences have been extensively used. The simian virus SV40 large T antigen, which is predominantly nuclear protein, contains a sequence with five basic amino acids (^{127}Lys-Lys-Lys-Arg-Lys^{131}). Point mutation experiments revealed that Lys^{128} is essential for the transportation of the large T antigen into the nucleus (Kalderon et al., 1984).

In the present work the effect of the palmitoylated $SV_{126\text{-}133}(Ser^{128})$ peptide (Pal-SV) on the conformation and associative behaviour of ODN was studied.

As the AFM makes topography of the surface, to successfully investigate peptides and oligonucleotides the samples had to be diluted at least 1000-fold from the concentrations used for spectroscopic measurements and dried on mica surface.

In order to visualize the complex formation between Pal-SV peptide and an 18 mer, GFP targeted ODN, atomic force microscopic images of Pal-SV, oligonucleotide, and their mixture at molar ratios of $r_M = 1$ and $r_M = 20$ have been recorded. All the images were recorded in air in AC mode with the cantilever driven at its resonant frequency of 70 kHz.

On the left column of Fig. 8. the 1 x 1 μm^2 topography of 400 nM Pal-SV peptide dried on mica surface is presented. The peptides appear as randomly spread 0.4 ± 0.1 nm high

spots. Clean surface of mica are distinguishable, proving that such concentration of peptide was convenient for AFM studies. Further diluted peptide presented the same patches, but with increased free mica surfaces between them.

The oligonucleotides were studied at a concentration of 20 nM. As they were dried on the mica surface they presented around 1 μm long fibrous structures, with an average height of 1.2 ± 0.3 nm (Fig. 8. right column). In most cases they overlapped and formed network.

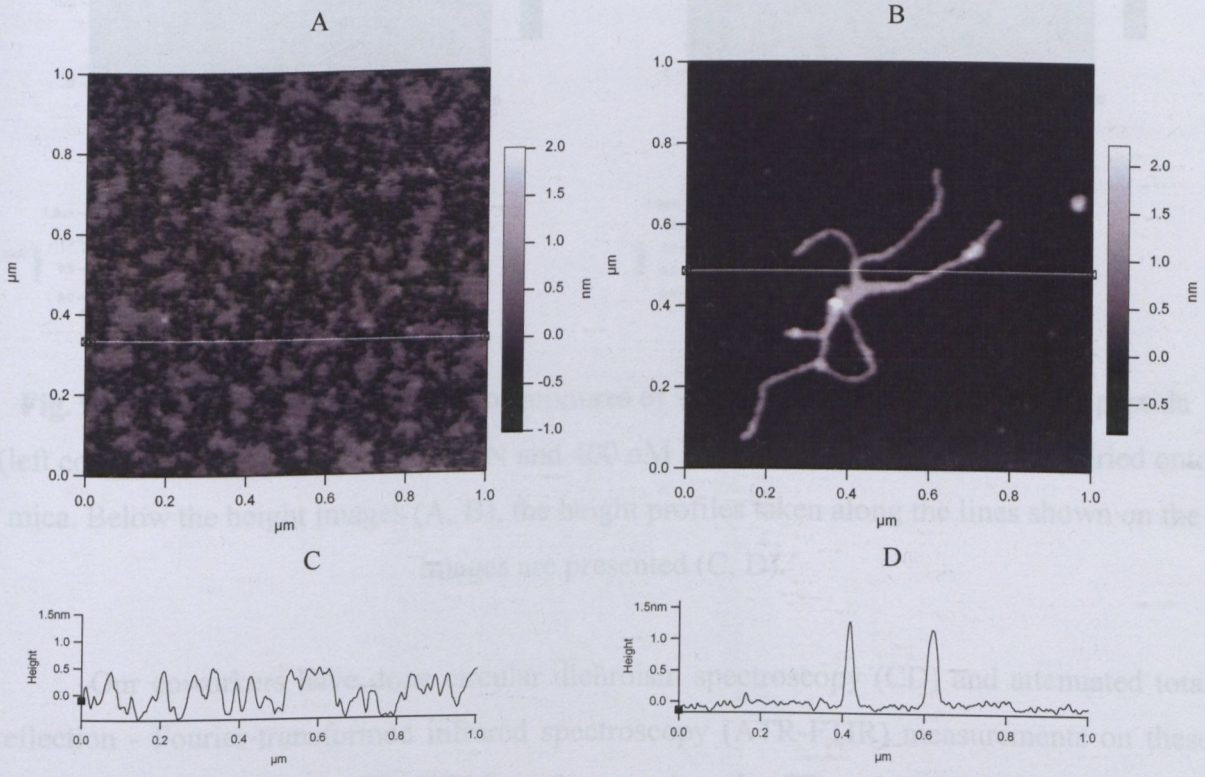

Fig. 8. 1 x 1 μm^2 height image of 400 nM Pal-SV peptide (left column) and 20 nM ODN (right column) dried on mica. Below the height images (A, B), the height profiles taken along the lines shown on the images are presented (C, D).

In the case of r_M = 1 the ODN and the peptide did not form complexes and they appeared separately on the AFM images (Fig. 9. left column). At r_M = 20 the ODN fibers were coated by the peptide (Fig. 9. right column). Due to the strong electrostatic interaction between the peptides and ODNs, the complex could be visualized even in the case of highly diluted samples used for AFM studies.

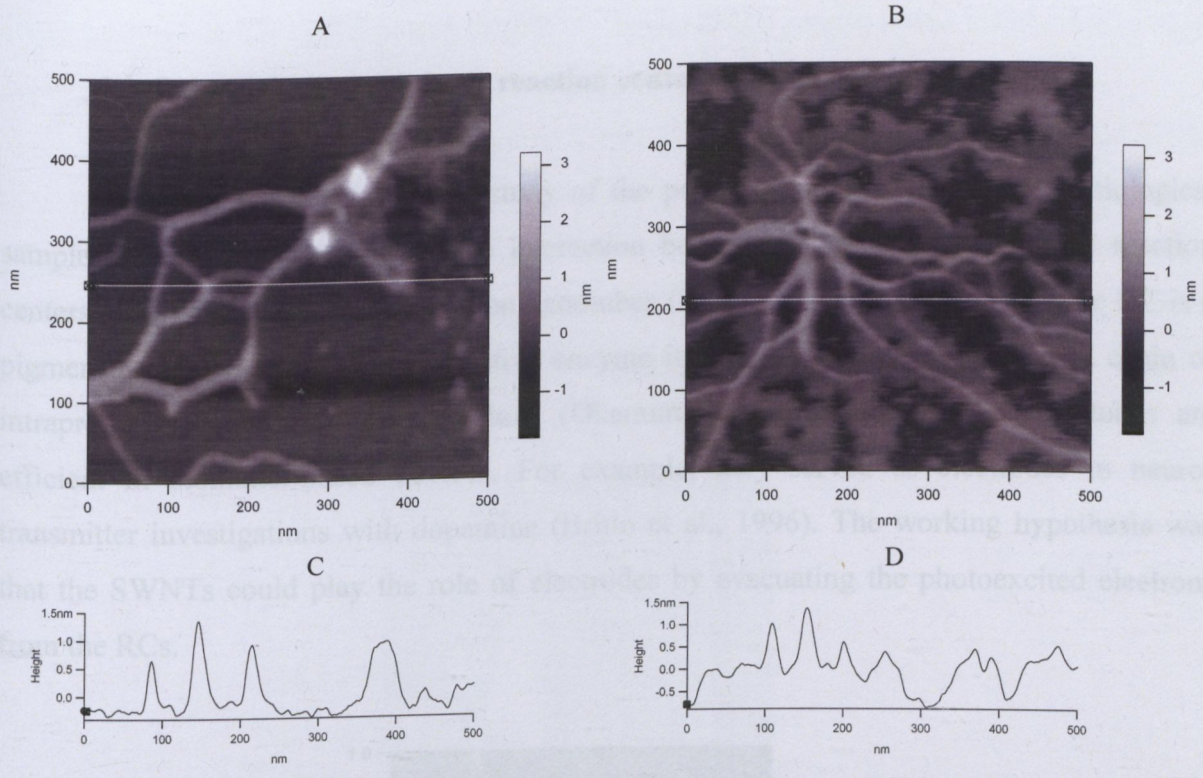

Fig. 9. 500 x 500 nm^2 height image of mixtures of 20 nM ODN and 20 nM Pal-SV peptide (left column), respectively 20 nM ODN and 400 nM Pal-SV peptide (right column) dried onto mica. Below the height images (A, B), the height profiles taken along the lines shown on the images are presented (C, D).

Our coworkers have done circular dichroism spectroscopy (CD) and attenuated total reflection - Fourier-transformed infrared spectroscopy (ATR-FTIR) measurements on these peptide - ODN complexes. The AFM results complete the CD and FTIR data, proving that this technique can serve well as a complementary method for biological sample investigations.

This part of the work was published in the *Archives of Biochemistry and Biophysics* (see Publication List No.II).

3.3. Bacterial photosynthetic reaction centers and carbon nanotubes

An exciting subject was the study of the possible complex formation of biological samples and synthetic products. The interaction between bacterial photosynthetic reaction centers (RCs) and single-walled carbon nanotubes (SWNTs) have been studied. The RC is a pigment protein complex, a redox-active enzyme in which light energy initiates a chain of intraprotein electron transport reactions (Okamura et al., 2000). Carbon nanotubes are efficient in biomatter-based devices. For example, they served as electrodes in neuro-transmitter investigations with dopamine (Britto et al., 1996). The working hypothesis was that the SWNTs could play the role of electrodes by evacuating the photoexcited electrons from the RCs.

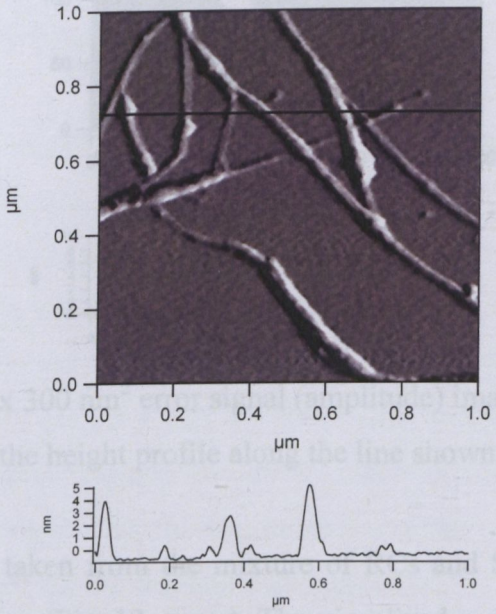

Fig. 10. 1 x 1 μm^2 error signal (amplitude) image of surface dried SWNTs and the height profile along the line shown on the image.

The RCs, the SWNTs and the complex of them dried on mica surface was imaged, using the ability of the AFM to image surface dried samples with high resolution. The error signal (amplitude) images of the samples are presented, in order to prove their usefulness. The SWNTs showed 1 nm high fibrous-like structures and as they dried on the mica surface they

assembled in bundles of 3-5 pieces (Fig. 10.). On the height profile it was visible that in those regions the height of the structures increased up to 4 - 5 nm.

The surface-dried RCs presented small, uniformly spread spots with an average height of 9 ± 1 nm. Making a high resolution picture of them revealed some surface structures (Fig. 11.). The error signal (amplitude) image showed single proteins (Fig. 11. top right corner) and in certain cases even dimers of them. The contact region of the dimer forming proteins was observable on the image (Fig. 11. center).

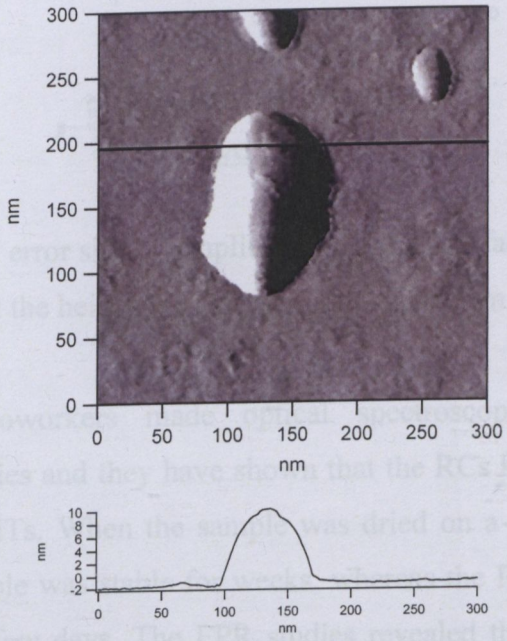

Fig. 11. 300 x 300 nm^2 error signal (amplitude) image of dried RC protein and the height profile along the line shown on the image.

On the images taken from the mixture of RCs and SWNTs, free proteins were also observable on the surface (Fig. 12. spots). The visualized carbon nanotubes were coated with proteins (Fig. 12.). From the height profile it could be derived that the RCs were sitting on the nanotubes forming a complex with an average height of 15 ± 2 nm. There were regions of the nanotubes with even double protein coating.

The height of the RC/SWNT complex corresponded to the sum of the height of each component. The AFM results had strengthened the idea that the RCs were attached to the nanotubes forming stable complexes.

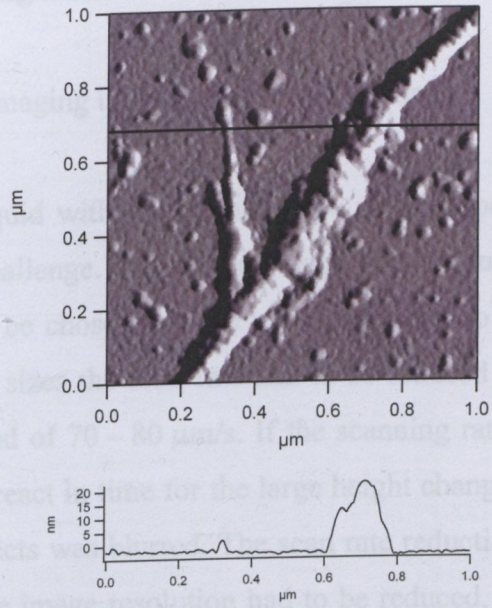

Fig. 12. 1 x 1 μm^2 error signal (amplitude) image of surface dried RC/SWNT complex and the height profile along the line shown on the image.

Our coworkers made optical spectroscopy and electron paramagnetic resonance (EPR) studies and they have shown that the RCs kept their photosynthetic activity after binding to SWNTs. When the sample was dried on a surface the decay kinetics were biphasic and the sample was stable for weeks, whereas the RCs alone in dried form had lost their activity after a few days. The EPR studies revealed that there was a direct electronic communication between the RCs and SWNTs. This special electronic property opens the possibility of different practical applications in microelectronics or in energy conversion and storage. It have been proven that the nanotubes serve not only as a perturbation factor, but also as a stabilizing agent for the reaction center proteins.

This part of the work was published in the *Journal of Physical Chemistry B* (see Publication List No.I).

3.4. Cell investigations

3.4.1. Imaging in liquid; parameter settings

Working in liquid with the atomic force microscope is a difficult task and imaging living cells is a real challenge. The cells are huge objects from the point of view of the AFM, large scan size had to be chosen and the main parameter to take care was the scanning rate. Because of large scan sizes the scan rate had to be reduced to values of 0.5 – 0.6 Hz, which meant a scanning speed of 70 – 80 μm/s. If the scanning rate was too high (above 1 Hz) the feedback loop cannot react in time for the large height changes and the image had stripes and the contour of the objects was blurred. The scan rate reduction implied the increase of image acquisition time, so the image resolution had to be reduced, by decreasing the scan points to 256 x 256, in order to make one image in 7 – 8 minutes.

In liquid the resonant frequency of the cantilever was shifted toward low values and usually they were driven at their first harmonic. The gain values were lower than those used in air, because of fluid viscosity, softness of the samples and low force constants of the cantilevers. For example, a Bio-Lever type cantilever supported integral gain values of 2 – 3 during cell imaging in liquid in contact mode. In the case of AC mode imaging with the Bio-lever mini type cantilever, the integral gain values could have been risen up to 7 – 8.

During the measurement both the trace and retrace images were recorded and compared to eliminate possible artifacts caused by the scan speed and the cantilever shape. They were found identical, therefore only one of them is presented.

3.4.2. Imaging fixed cells

The fixed epithelial cells (MDCK) were imaged in buffer solution in AC mode. The dominant feature observed with the AFM was the high central part of the cell, identified as the nucleus (Fig. 13.). The error signal image (in this case the amplitude) provided a detailed picture of the surface of the cells. It also showed the cell boundaries and cell-to-cell

contacts. The observed maximum cell height was ~3 μm and their size had been in the range of 30 – 40 μm, respectively.

The true cell height differed from this value, because here fixed cells were imaged and beside this, the cells were indented to a certain level by the AFM tip. The indentation could be calculated from force curves measured on the cells. From these data the real cell height could be estimated. But if the measuring conditions and imaging parameters were the same and only the changes of the cell morphology were followed, there was no need to estimate the real height of the cells.

Using the inverted optical microscope, on which the AFM system was built, simultaneously fluorescence measurements were possible. This opens the possibility to study the same cells with two independent techniques in the same time, providing information not only from their surface, but also from the localization of junction forming proteins.

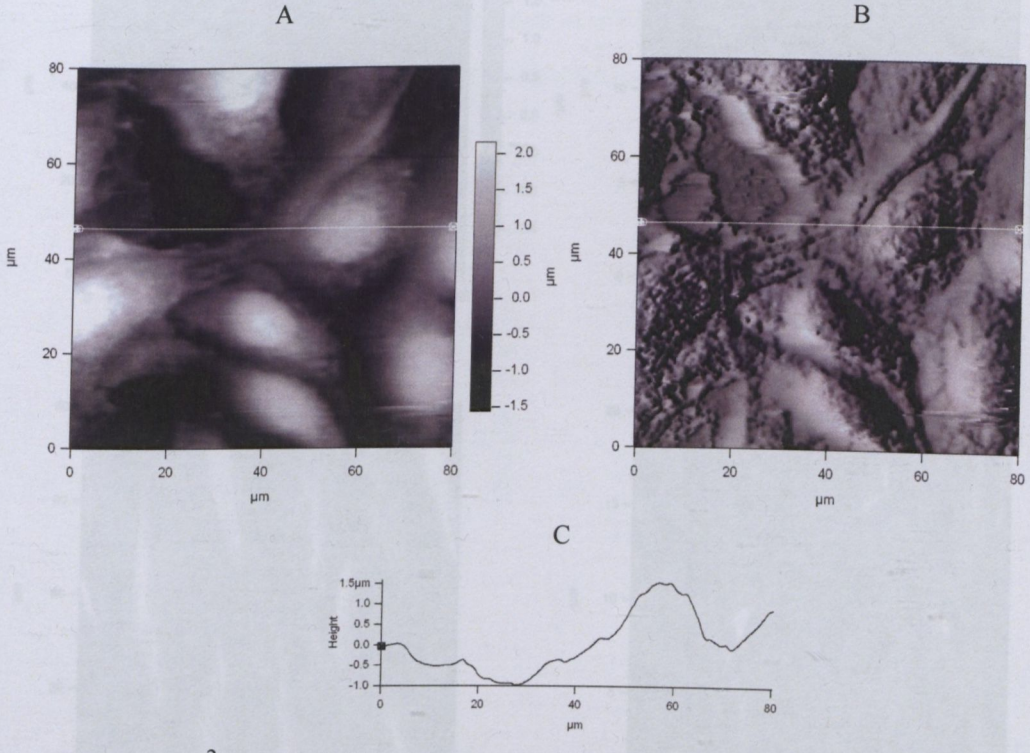

Fig. 13. 80 x 80 μm^2 height (A) and (B) error signal (amplitude) images of fixed MDCK cells. Below the height image, the height profiles taken along the line shown on the images is presented (C).

3.4.3. Imaging living cells: cytoskeleton and surface features

The AFM's possibility to work in liquid environment and especially the design of the MFP-3D type AFM made possible to study living cells in Petri dishes, in their physiological circumstances. The first problem to overcome was the sample stability. As the AFM tip comes into physical contact with the cells it could happen that they had been pushed away by the tip. Fortunately the studied cell types adhered sufficiently to the surface of the Petri dish to support this disturbance and the introduced extracellular factors had not influenced the cell adherence to the surface.

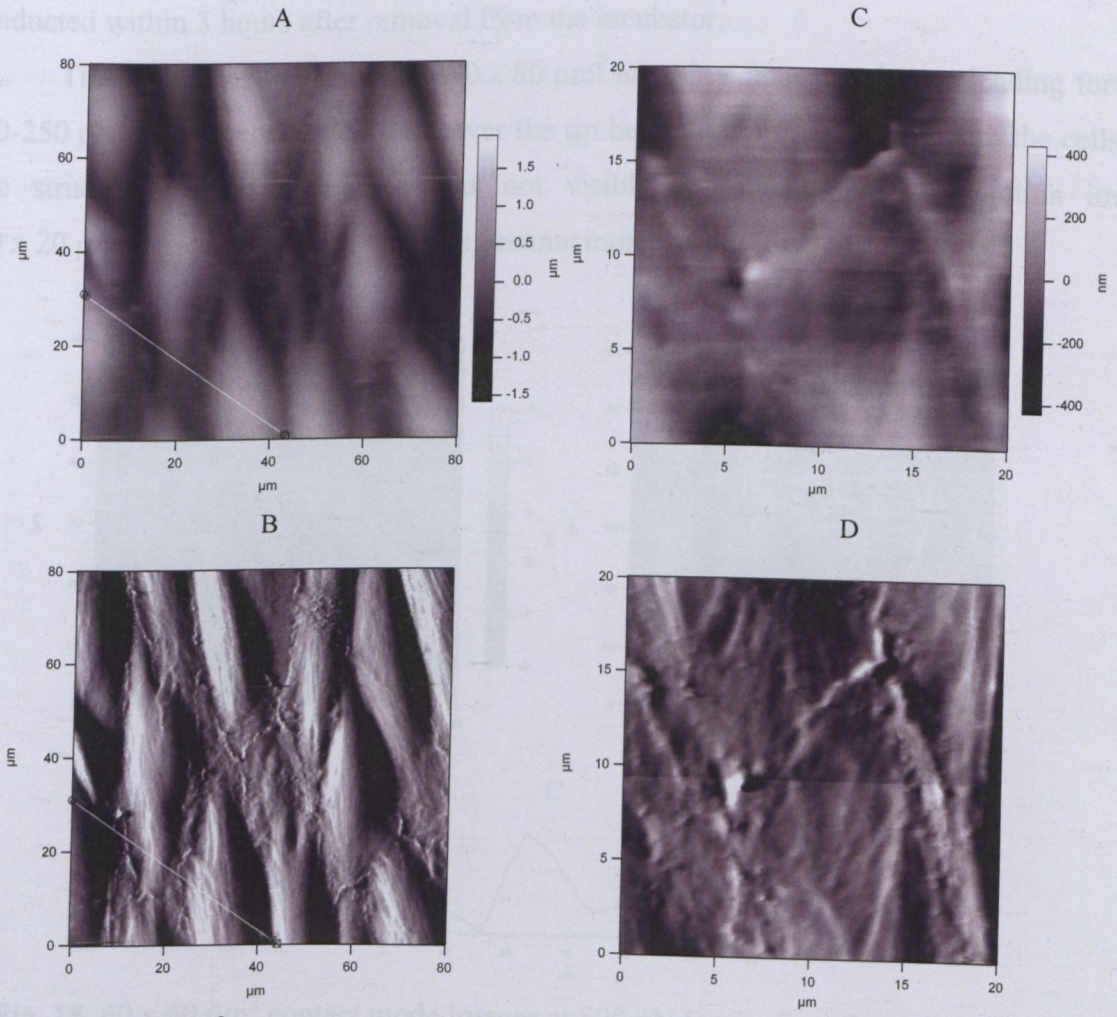

Fig. 14. 80 x 80 µm^2 and 20 x 20 µm^2 contact mode images at low force of confluent living cerebral endothelial cells. Height (A, C) and error signal (deflection) images (B, D).

The vascular endothelial cells in their native environment are exposed to continuous collision with blood cells, therefore they are mechanical resistant supporting the imaging force of the AFM, if the value of it is kept below 1 nN (Pesen and Hoh, 2005b). In Petri dishes they form a uniform, confluent monolayer and usually do not overlap, therefore any change in their shape and size is visible and can be quantified from the AFM topographies.

The Petri dish with the confluent GP8 rat cerebral endothelial cell culture was mounted on the sample stage of the AFM. The cells were imaged at 31 °C in a closed chamber. Before the measurement started the system was let to reach thermal stability. When the deflection change was maximum 20 mV in 10 minutes, corresponding to 50 pN force change during image acquisition, the experiments could be started. The experiments were conducted within 3 hours after removal from the incubator.

The surface of the cells on a 80 x 80 μm^2 area, in contact mode at a loading force of 200-250 pN, have been imaged. However the tip being in constant contact with the cells, the fine structure of the membrane was not visible. By making high resolution images (20 x 20 μm^2 area) the cell-cell contacts became more visible (Fig. 14.).

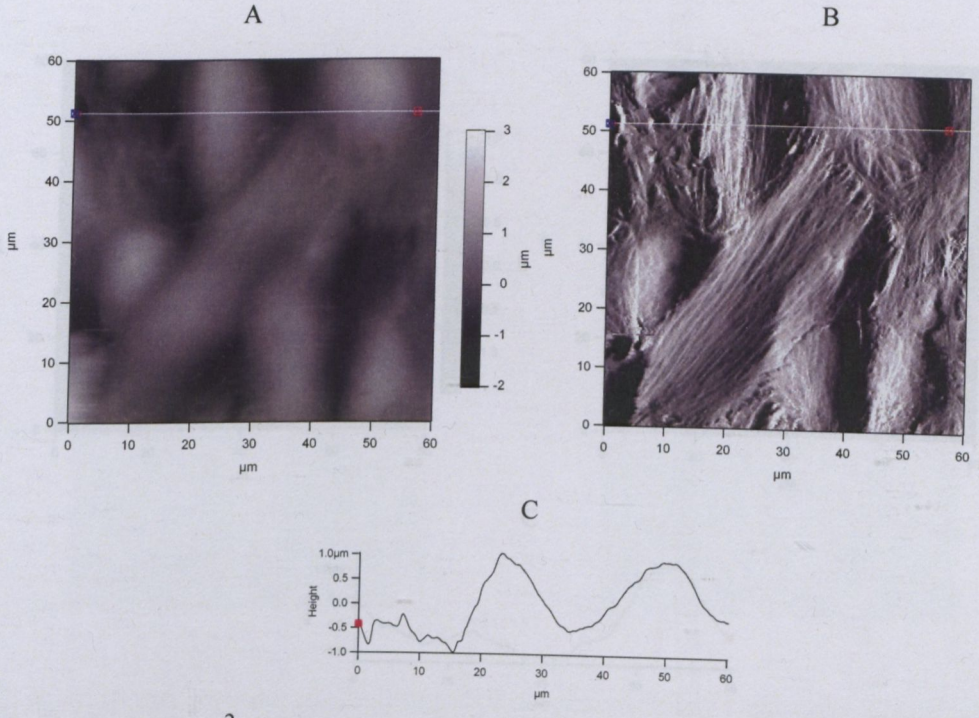

Fig. 15. 60 x 60 μm^2 contact mode images at 500 pN force of confluent living cerebral endothelial cells. Height (A), error signal (deflection) images (B) and the height profile along the line shown on the image (C).

By raising the loading force to 500 - 600 pN an insight look of the cells was obtained, which meant that by pressing the soft membrane on the underlying cytoskeleton structure, the latter became visible on the images (Fig. 15.). As it could be observed in detail on the error signal image (deflection) the cytoskeleton presented fibrous, branching structures (Han et al., 2004). In this way the harder structures of the cells have been imaged and it provided the opportunity to follow not only surface changes, but also changes happening at the membrane underlying region of the cells, induced by extracellular stimuli. In the case when the loading force was over 1 nN the tip penetrated the cell membrane and ripped it. No presentable images could be made.

As a comparison, the much stiffer epithelial cells (MDCK) supported forces up to 1.5 - 2 nN without any damages. The cells had rounded shape, and their surface was found to be rougher than in the case of endothelial cells. On these pictures different regions of the cells were more distinguishable and the cell-cell contacts were visible then in the case of CEC topographies (Fig. 16.).

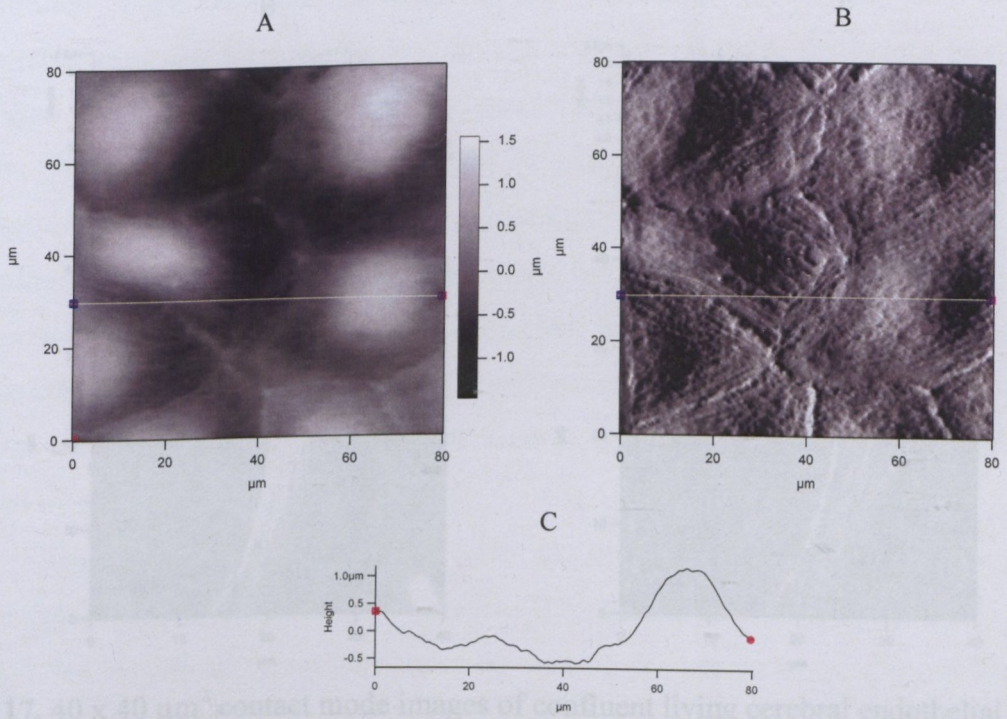

Fig. 16. 80 x 80 μm^2 contact mode images at 1.5 nN force of confluent living epithelial cells. Height (A), error signal (deflection) images (B) and the height profile along the line shown on the image (C).

3.4.4. Effect of mannitol on living cerebral endothelial cells

Surface topographies of living, confluent CECs in their normal medium with a loading force of ~600 pN and a scan rate of 0.6 Hz were recorded (Fig. 17.). Without moving neither the instrument, nor the Petri dish the solution was changed to a 10% (0.55 M) mannitol containing one. This is the relevant concentration of mannitol used in clinical applications.

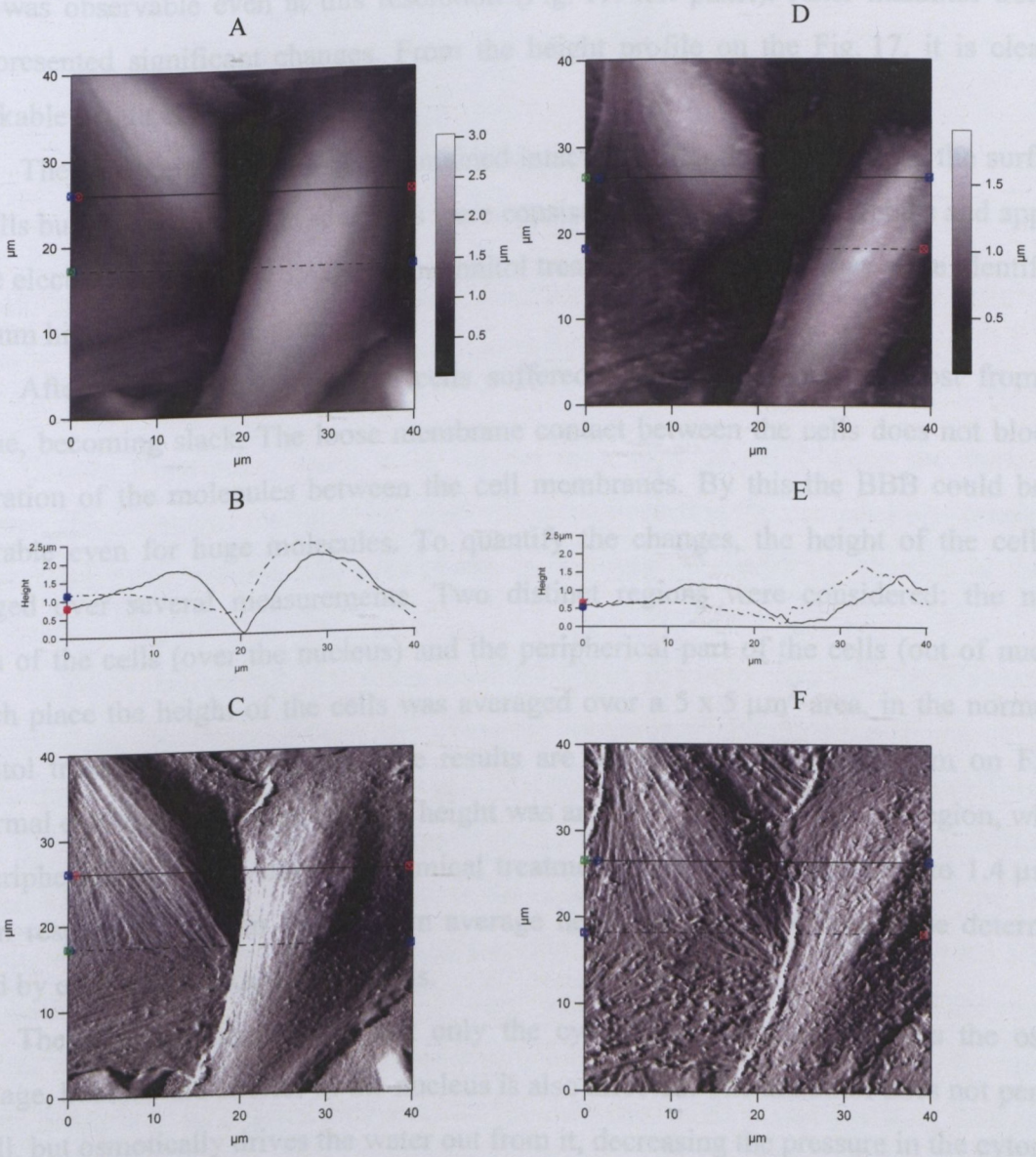

Fig. 17. 40 x 40 µm^2 contact mode images of confluent living cerebral endothelial cells before (left column) and after mannitol treatment (right column). Height images (A, D), height profiles along the line shown on the images (B, E) and error signal (deflection) images (C, F), respectively.

At this concentration the mannitol has a hyperosmotic effect, so the cells lose liquid. After the mannitol had its effect (30 minutes) the same cells were imaged with the same measuring parameters. Usually the new image was shifted with 5 - 10 μm related to the original one. This could be easily corrected from software by adjusting the x and y offset of the next image and the correlation of the consecutive images was possible.

The living cerebral endothelial cells had elongated shape and the contact between them was observable even at this resolution (Fig. 17. left panel). After mannitol treatment they presented significant changes. From the height profile on the Fig. 17. it is clear that remarkable height changes occurred.

The cytoskeleton of the cells remained intact, but after the treatment on the surface of the cells bumps appeared. These bumps were consistent in repeated experiments and appeared on the electron microscopic images of mannitol treated cells, as well. They were identified as ~100 nm high cytoplasmic protrusions.

After mannitol treatment the cells suffered an osmotic shock and lost from their volume, becoming slack. The loose membrane contact between the cells does not block the penetration of the molecules between the cell membranes. By this the BBB could became penetrable even for huge molecules. To quantify the changes, the height of the cells was averaged over several measurements. Two distinct regions were considered: the nuclear region of the cells (over the nucleus) and the peripherical part of the cells (out of nucleus). In each place the height of the cells was averaged over a 5 x 5 μm^2 area, in the normal and mannitol treated cases separately. The results are presented in graphical form on Fig. 18. At normal conditions the observed cell height was around 2 μm in the nuclear region, whereas the periphery had 1 μm. After the chemical treatment these values decreased to 1.4 μm and 0.5 μm respectively. From this data an average height change of 40% can be determined, caused by osmotic shrinkage of the cells.

These results suggest that not only the cytoplasm of the cell suffers the osmotic shrinkage, but also the interior of the nucleus is also affected. The mannitol does not penetrate the cell, but osmotically drives the water out from it, decreasing the pressure in the cytoplasm. The excess pressure of the nucleus is equilibrated by liquid exclusion as well.

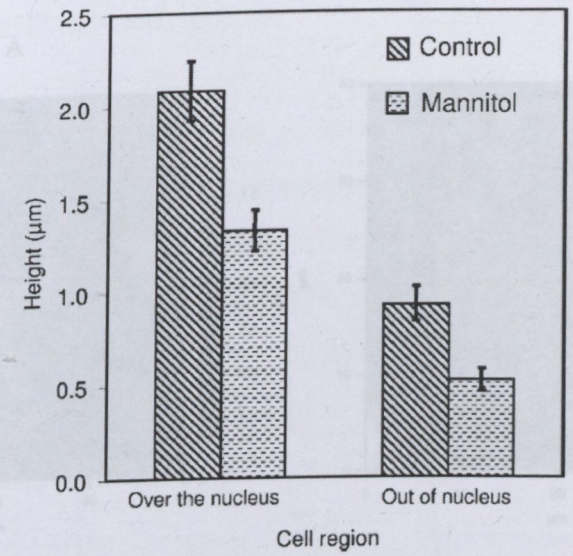

Fig. 18. The average thickness of the cells measured over the nucleus and at the peripherical region of the cell, in normal conditions and after mannitol treatment.

Control experiments were made on the same type of cells, when the same liquid exchange procedure was repeated, but from the second solution the mannitol was missing and to the cells their normal medium was given. In this case no significant changes of the cells were observed (Fig. 19.).

To prove the reversibility of the mannitol effect, it would have been good to continue the experiment by changing back the mannitol containing medium to that without it and observe the reversal of the changes. But even the sturdy endothelial cells of the BBB were not stable for such a long time and so many AFM scanning. To overcome this difficulty a reversed experiment was performed. After the cells were grown to confluency, the original medium was exchanged to that containing mannitol. The cells in the Petri dish were scanned, after one hour equilibration in the AFM. They exhibited the characteristics of the mannitol treatment, cell height bellow 1.5 µm and protrusions on the surface of the cell. By changing back the medium to its original composition, the cells recovered within one hour their original height of about 2 µm and the protrusions disappeared. These observations proved that the mannitol induced changes were reversible.

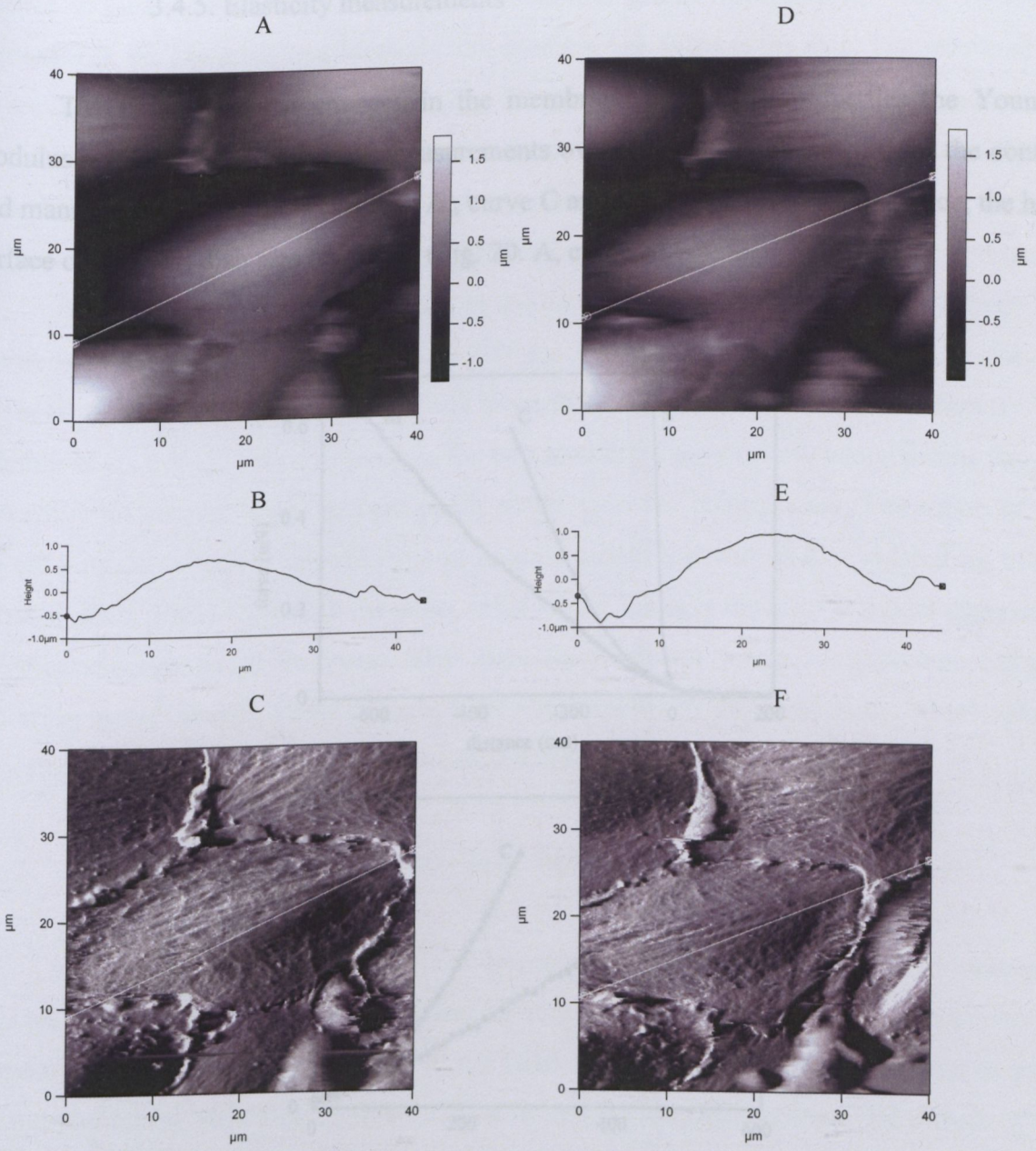

Fig. 19. 40 x 40 μm^2 contact mode images of confluent living cerebral endothelial cells before (left column) and after changing the solution, but without mannitol (right column). Height images (A, D), height profiles along the line shown on the images (B, E) and error signal (deflection) images (C, F), respectively. No significant changes could be observed.

This part of the work was published in the *European Biophysical Journal* (see Publication List No.III).

3.4.5. Elasticity measurements

To characterize the changes in the membrane mechanical properties the Young's modulus was determined by force measurements over the nucleus of the cell, for the control and mannitol treated cultures (Fig. 20. A., curve C and M respectively). As reference, the hard surface of the Petri dish was measured (Fig. 20. A, curve S).

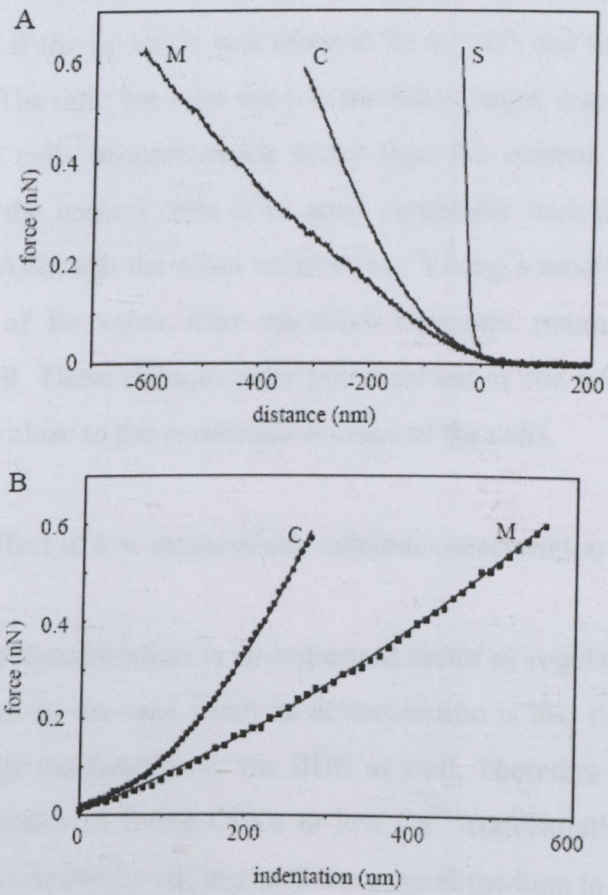

Fig. 20. Force curves on the Petri dish surface (S) and on endothelial cells before (C) and after (M) mannitol treatment. From the measured force versus distance curves (panel A) the force versus indentation curves were calculated (panel B, points) and the fits to the Hertz model are shown (panel B, continuous lines).

From these data the indentation of the cell membrane was calculated for both the control and mannitol treated cells (Fig. 20. B, curve C and M respectively). Using the model presented in the Materials and Methods, the equation was fitted to the data. The results of the fit are shown as continuous lines on the Fig. 20. panel B. As the figure shows, the indentation of the mannitol treated membrane is much larger, compared to the control. Apparently the mannitol treated membrane is much softer, which can be explained by the fact that the mannitol treatment removes a large part of the cell volume, but the surface remains constant.

The calculated Young's modulus, based on the theory mentioned in the Materials and Methods, was found to be 8.04 ± 0.12 kPa for the control and 0.93 ± 0.04 kPa for the mannitol treated cells, if the tip angle was taken to be $\alpha = 45°$ and the Poisson ration $\mu = 0.4$ (Mathur et al., 2001). The ratio between the two moduli is larger than 8, which means that the hyperosmotic stressed cells become much softer than the control ones. The value of the Young's modulus for the control cells is in good agreement with that calculated by others (Mathur et al., 2001). Although the exact value of the Young's modulus is model dependent, the dramatic change of its value after mannitol treatment points to important changes occurring inside the cell. These changes were not observed by the AFM study, which detects only structural changes close to the membrane surface of the cells.

3.4.6. Effect of low extracellular calcium concentration on living cells

The calcium ion concentration is an important factor of regular function of individual cells and whole systems. In the case when its concentration is low the cells cannot function properly and can damage the function of the BBB as well. Therefore it is important to study the morphological responses of living CECs to low Ca^{2+} concentrations. The effects of the low concentration are reversible by adding back the normal medium to the cells.

The imaging parameters and conditions were the same as in the case of the experiment with mannitol.

The AFM provides the possibility of direct observation of cell's morphological responses in time. To avoid possible degradation effects of the cells during the long AFM examination, it was chosen to monitor the recovery process after being exposed to low extracellular Ca^{2+} concentrations. Before the experiment the confluency of the immortalized

human brain endothelial cell culture (hCMEC/D3) was checked with optical microscope and the solution was exchanged to low calcium containing one. After the cells being 60 minutes under low calcium circumstances the Petri dish was mounted on the sample stage of the AFM and images were taken.

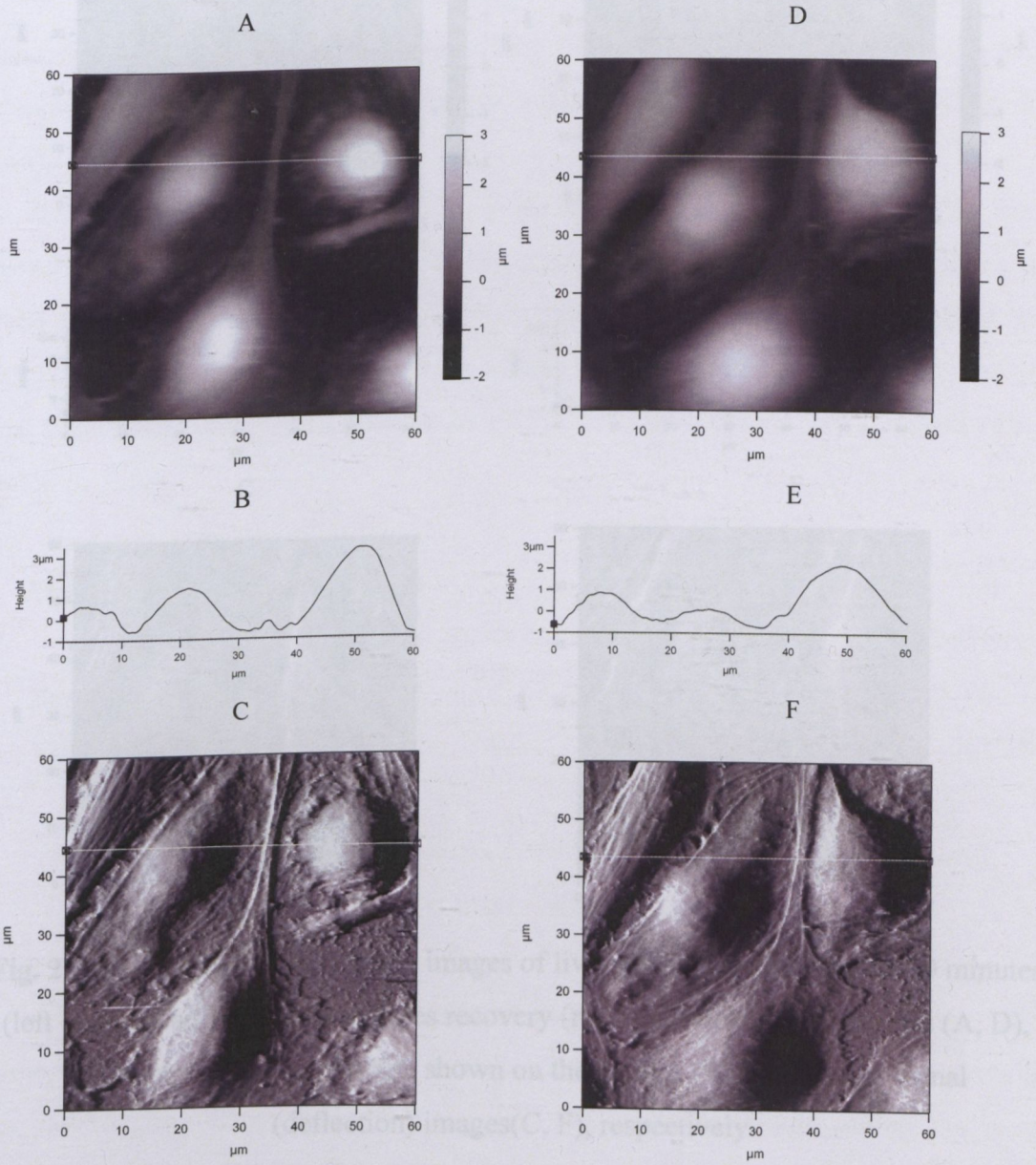

Fig. 21. 60 x 60 μm^2 contact mode images of living endothelial cells 90 minutes in calcium deficient conditions (left column) and after 15 minutes recovery (right column). Height images (A, D), height profiles along the line shown on the images (B, E)and error signal (deflection) images (C, F), respectively.

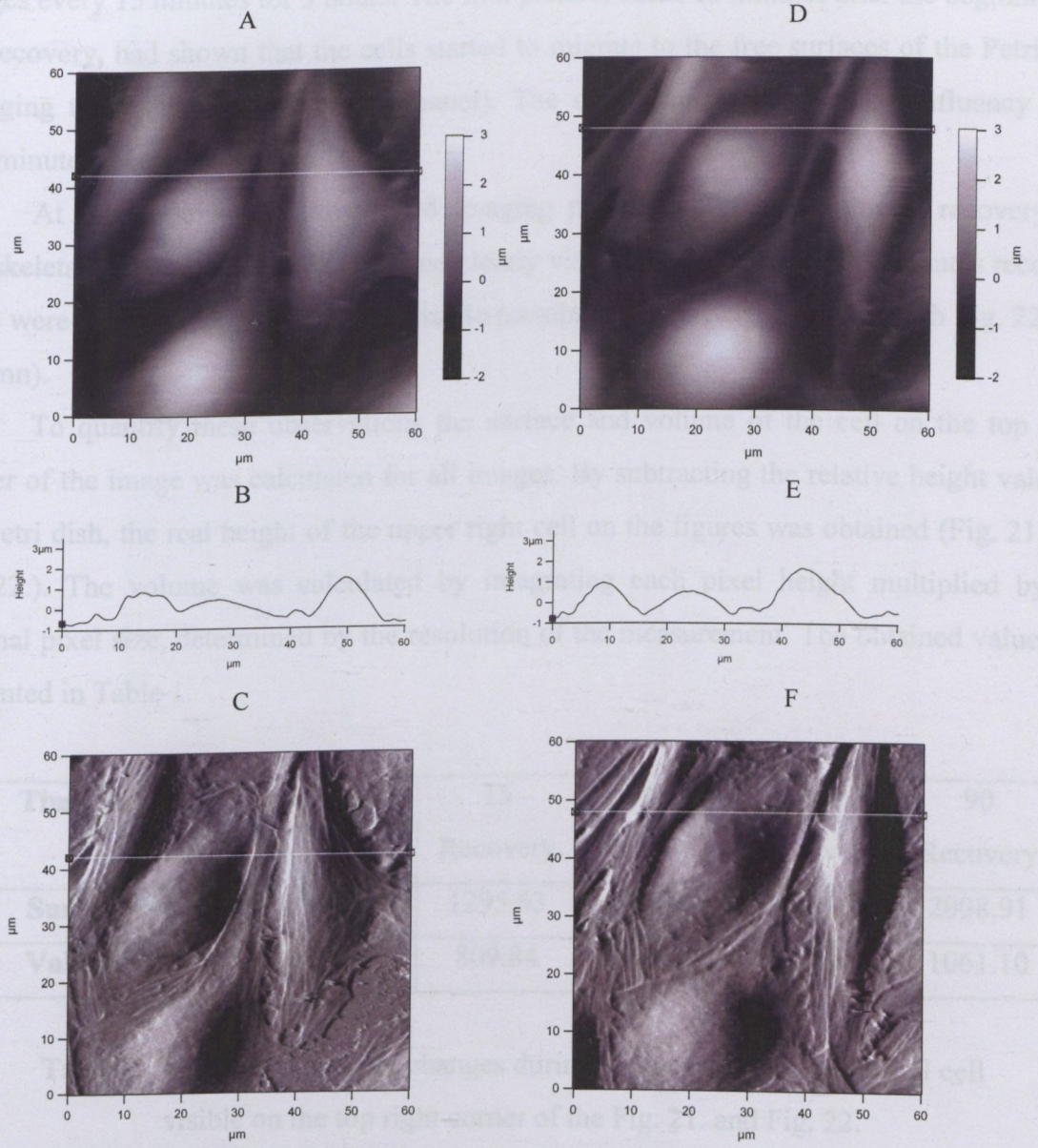

Fig. 22. 60 x 60 μm^2 contact mode images of living endothelial cells after 90 minutes (left column) and after 150 minutes recovery (right column). Height images (A, D), height profiles along the line shown on the images (B, E) and error signal (deflection) images(C, F), respectively.

On the Fig. 21. clear surfaces of the Petri dish are visible proving that the cell culture dissociated, accompanied with the disruption of the cell-cell junctions. The cells had increased height and rounded morphology. After the image acquisition the solution was

changed back to the normal medium and the recovery process was monitored recording images every 15 minutes for 3 hours. The first picture, taken 15 minutes after the beginning of the recovery, had shown that the cells started to migrate to the free surfaces of the Petri dish changing their shape (Fig. 21. right panel). The cell culture regained its confluency after 150 minutes recovery.

At the same loading force and imaging parameters after 90 minutes recovery the cytoskeletal structure of the cells became clearly visible, whereas at only 15 minutes recovery there were less cytoskeletal elements visible (compare Fig. 21. right column with Fig. 22. left column).

To quantify these observations the surface and volume of the cell on the top right corner of the image was calculated for all images. By subtracting the relative height value of the Petri dish, the real height of the upper right cell on the figures was obtained (Fig. 21. and Fig. 22.). The volume was calculated by integrating each pixel height multiplied by the original pixel size, determined by the resolution of the measurement. The obtained values are presented in Table 1.

Time (minutes)	90 Ca-	15 Recovery	45 Recovery	60 Recovery	90 Recovery
Surface (μm^2)	1001.75	1295.63	1397.03	1764.64	2008.91
Volume (μm^3)	594.40	809.84	813.88	963.71	1061.10

Table 1. Surface and volume changes during recovery of the endothelial cell visible on the top right corner of the Fig. 21. and Fig. 22.

After addition of calcium a significant increase in the average cell volume (63.6%) was detectable (Table 1.). Nearly the same increase could be observed in the average cell surface too (61.7%). This shows that the cells are taking up liquid during the recovery. The low calcium concentration induced a volume and surface decrease of the cells, which was reversible after adding back the calcium. There was no information about where the extra membrane lipids were during the decrease. After 90 minutes recovery there was no further significant increase in cell surface and volume.

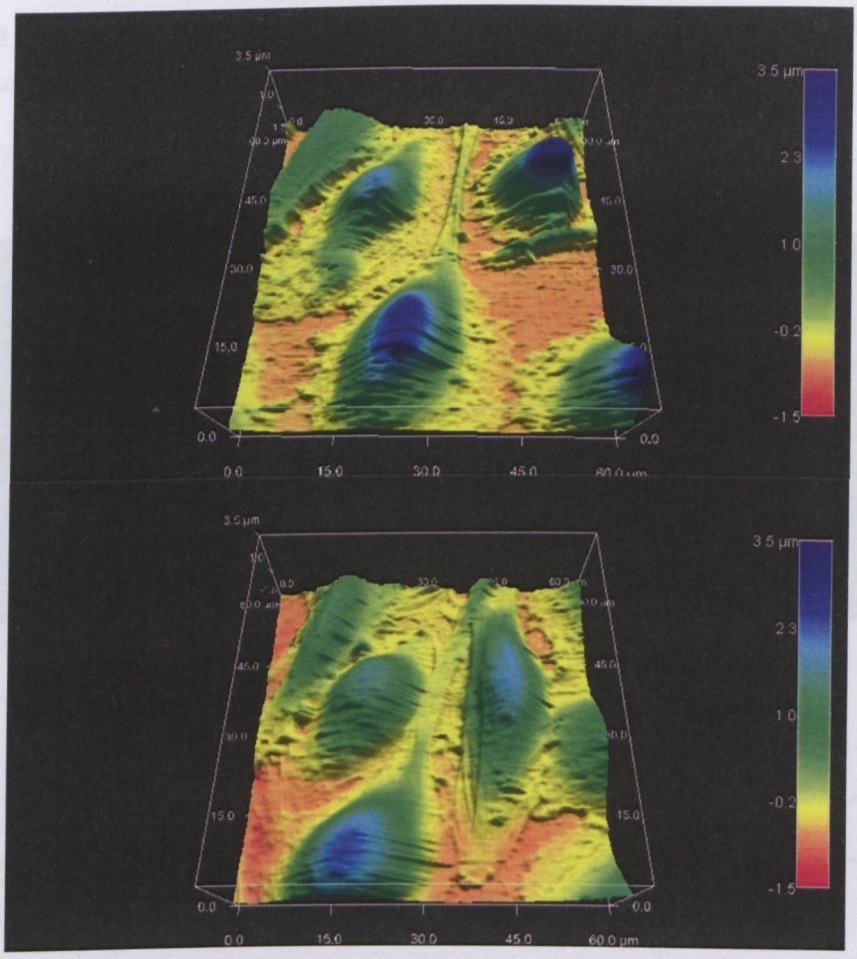

Fig. 23. Pseudo-3D presentations of the images presented on Fig. 21. and Fig. 22. left panel.

For a better visualization of the recovery processes pseudo-3D images were generated from the collected AFM data (Fig. 23.). The broken junctions between the cells and the decreased surface were more accentuated. On these pictures the surface of the Petri dish was distinct and the height changes were easily distinguishable.

As a control, the same experiments were conducted on 3T3/L1 fibroblast cells, which are not expressing junction forming proteins in their membrane. The same experiment was conducted as in the case of endothelial cells, but the fibroblasts had not responded with morphological changes to extracellular Ca^{2+} removal and readdition (Fig. 24.).

After 50 minutes of being in calcium deficient conditions there was no free surface of the Petri dish detectable (Fig. 24. left column). On the images taken after adding back the normal medium no significant changes in the cell shape and size were observed (Fig. 24. right

column). This control assured that the observed changes of the CECs were strongly related to their junction-forming property.

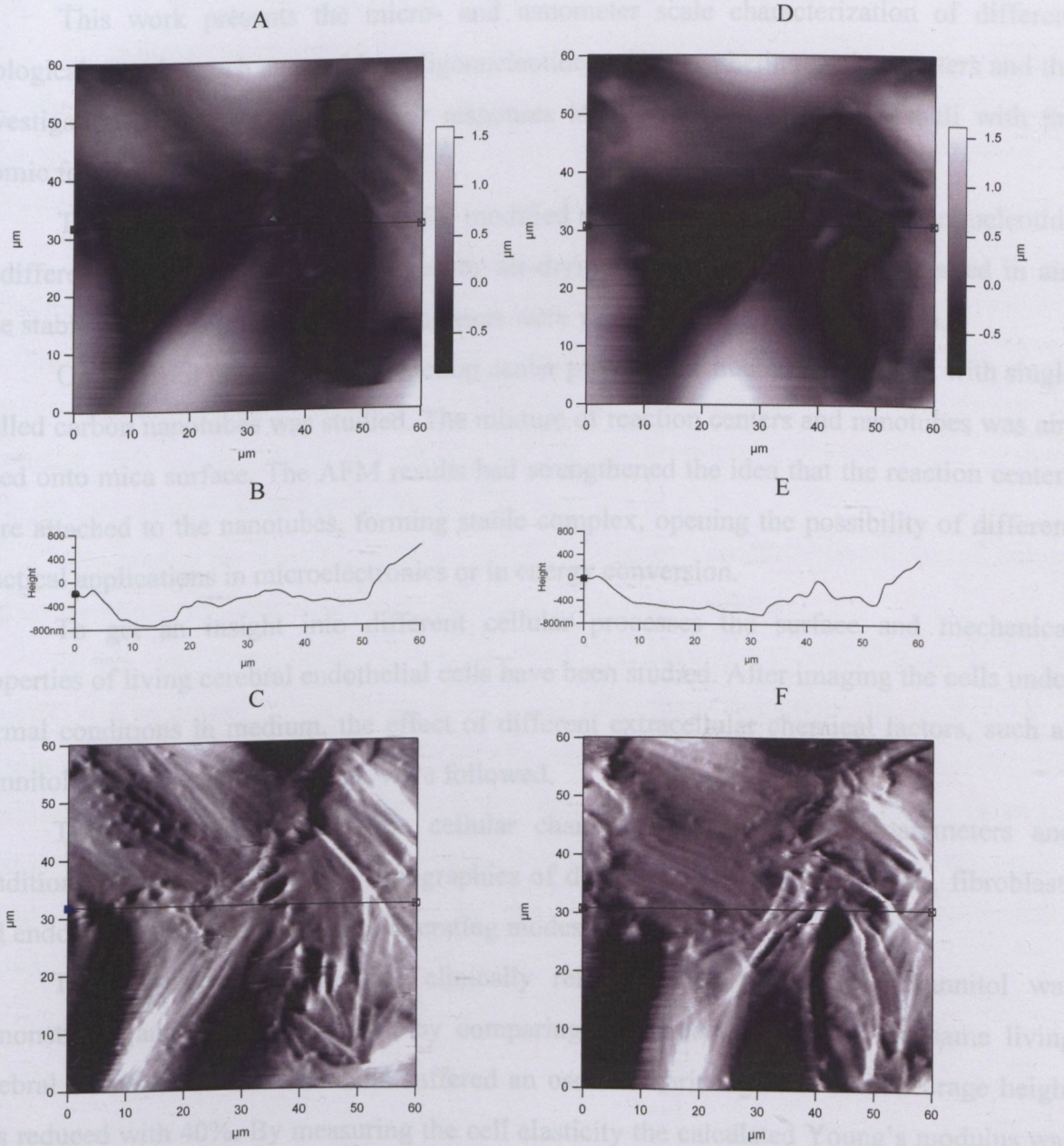

Fig. 24. 60 x 60 μm^2 contact mode images of fibroblast cells, 50 minutes in lack of calcium (left column) and 40 minutes recovery (right column). Height images (A, D), height profiles along the lines shown on the images (B, E) and error signal (deflection) images (C, F).

4. Conclusions

This work presents the micro- and nanometer scale characterization of different biological samples such as peptides, oligonucleotides, photosynthetic reaction centers and the investigation of living cells and their responses to different extracellular stimuli with the atomic force microscope.

The complexes formed by Pal-SV modified signal peptide and 18 mer oligonucleotide at different concentrations were studied by air-drying onto mica surface and imaged in air. The stable peptide-oligonucleotide complexes were visualized with high resolution.

On bacterial photosynthetic reaction center proteins the interaction of them with single walled carbon nanotubes was studied. The mixture of reaction centers and nanotubes was air-dried onto mica surface. The AFM results had strengthened the idea that the reaction centers were attached to the nanotubes, forming stable complex, opening the possibility of different practical applications in microelectronics or in energy conversion.

To get an insight into different cellular processes the surface and mechanical properties of living cerebral endothelial cells have been studied. After imaging the cells under normal conditions in medium, the effect of different extracellular chemical factors, such as mannitol and low level of calcium, were followed.

To successfully monitor the cellular changes first the imaging parameters and conditions were set by recording topographies of different cell types (epithelial-, fibroblast- and endothelial cells) with different operating modes, in liquid.

The hyperosmotic effect of clinically relevant concentrations of mannitol was demonstrated and followed in time by comparing subsequent images of the same living cerebral endothelial cells. The cells suffered an osmotic shrinkage and their average height was reduced with 40%. By measuring the cell elasticity the calculated Young's modulus was found to be 8.04 ± 0.12 kPa for the control and 0.93 ± 0.04 kPa for the mannitol treated cells. The ratio between the two moduli was larger than 8, which meant that the hyperosmotic stressed cells became much softer than the control ones.

The changes observed with AFM might contribute to better understanding of the effect of opening the blood brain barrier by mannitol. Osmotic stress-induced volume changes,

observed in the presented experiments, might also contribute to the permeability increase, especially as the molecules forming the junctional complex are connected to the actin cytoskeleton. These observations predict that the opening of the blood brain barrier happens by the transient increase of the intercellular space between the endothelial cells.

Control experiments were made on the same type of cells. The same liquid exchange procedure was repeated, but from the second solution the mannitol was missing, and to the cells their normal medium was given. In this case no significant morphological changes of the cells were observed.

Another process to follow was the effect of the calcium depletion on cerebral endothelial cells. After reducing the extracellular calcium concentration, in the initially confluent cell culture islands were observable and the surface of the Petri dish became visible. The junctions between the cells had broken and the volume and surface of the cells decreased. Changing back the medium to the normal one the culture regained its confluency, and the cells got their original form and shape after 150 minutes.

As a control the same experiment was effectuated on a confluent fibroblast cell culture and no significant changes were observed after changing the medium.

In this work it was presented that the atomic force microscope is a very useful tool in biology and medicine. It can be used as a complementary technique for other type of measurements on dried biological samples. It can work in liquid by studying biological samples near their physiological state. High resolution images of living cells can be made. Beside single image acquisition the AFM can even serve as a unique tool to monitor morphological and mechanical changes in time of the same living cells upon extracellular stimuli.

5. Reference List

1. Bennink,M.L., D.N.Nikova, K.O.van der Werf, and J.Greve. 2003. Dynamic imaging of single DNA-protein interactions using atomic force microscopy. *Analytica Chimica Acta* 479:3-15.

2. Berdyyeva,T., C.D.Woodworth, and I.Sokolov. 2005. Visualization of cytoskeletal elements by the atomic force microscope. *Ultramicroscopy* 102:189-198.

3. Binnig,G., C.F.Quate, and C.Gerber. 1986. Atomic force microscope. *Physical Review Letters* 56:930-933.

4. Braet,F., R.deZanger, and E.Wisse. 1997. Drying cells for SEM, AFM and TEM by hexamethyldisilazane: a study on hepatic endothelial cells. *Journal Of Microscopy-Oxford* 186:84-87.

5. Britto,P.J., K.S.V.Santhanam, and P.M.Ajayan. 1996. Carbon nanotube electrode for oxidation of dopamine. *Bioelectrochemistry And Bioenergetics* 41:121-125.

6. Brus,C., E.Kleemann, A.Aigner, F.Czubayko, and T.Kissel. 2004. Stabilization of oligonucleotide-polyethylenimine complexes by freeze-drying: physicochemical and biological characterization. *Journal of Controlled Release* 95:119-131.

7. Bustamante,C. and C.Rivetti. 1996. Visualizing protein-nucleic acid interactions on a large scale with the scanning force microscope. *Annual Review Of Biophysics And Biomolecular Structure* 25:395-429.

8. Butt,H.J., K.H.Downing, and P.K.Hansma. 1990a. Imaging the membrane-protein bacterirhodopsin with the atomic force microscope. *Biophysical Journal* 58:1473-1480.

9. Butt,H.J., E.K.Wolff, S.A.C.Gould, B.D.Northern, C.M.Peterson, and P.K.Hansma. 1990b. Imaging cells with the atomic force microscope. *Journal Of Structural Biology* 105:54-61.

10. Cherny,D.I., A.Fourcade, F.Svinarchuk, P.E.Nielsen, C.Malvy, and E.Delain. 1998. Analysis of various sequence-specific triplexes by electron and atomic force microscopies. *Biophysical Journal* 74:1015-1023.

11. Chung,T.W., D.Z.Liu, S.Y.Wang, and S.S.Wang. 2003. Enhancement of the growth of human endothelial cells by surface roughness at nanometer scale. *Biomaterials* 24:4655-4661.

12. Costa,L.T., M.Kerkmann, G.Hartmann, S.Endres, P.M.Bisch, W.M.Heckl, and S.Thalhammer. 2004. Structural studies of oligonucleotides containing G-quadruplex motifs using AFM. *Biochemical And Biophysical Research Communications* 313:1065-1072.

13. Domke,J., S.Dannohl, W.J.Parak, O.Muller, W.K.Aicher, and M.Radmacher. 2000. Substrate dependent differences in morphology and elasticity of living osteoblasts investigated by atomic force microscopy. *Colloids And Surfaces B-Biointerfaces* 19:367-379.

14. Doolitle,N.D., M.E.Miner, W.A.Hall, T.Siegal, E.Jerome, E.Osztie, L.D.McAllister, J.S.Bubalo, D.F.Kraemer, D.Fortin, R.Nixon, and E.A.Neuwelt. 2000. Safety and efficacy of a multicenter study using intraarterial chemotherapy in conjunction with osmotic opening of the blood-brain barrier for the treatment of patients with malignant brain tumors. *Cancer* 88:637-647.

15. Engel,H.A. 1991. Biological applications of scanning probe microscopes. *Annual Review Of Biophysics And Biophysical Chemistry* 20:79-108.

16. Farkas,A., E.Szatmári, A.Orbók, I.Wilhelm, K.Wejszka, P.Nagyõszi, P.Hutamekalin, H.Bauer, H.C.Bauer, A.Traweger, and I.A.Krizbai. 2005. Hyperosmotic mannitol

induces Src kinase-dependent phosphorylation of beta-catenin in cerebral endothelial cells. *Journal of Neuroscience Research* 80:855-861.

17. Gergely,C., S.Bahi, B.Szalontai, P.Flores, P.Schaaf, J.C.Voegel, and F.J.G.Cuisinier. 2004. Human serum albumin self-assambly on weak polyelectrolyte multilayer films structurally modified by pH changes. *Langmuir* 20:5575-5582.

18. Goncalves,R.P., A.Bernadac, J.N.Sturgis, and S.Scheuring. 2005. Architecture of the native photosynthetic apparatus of Phaeospirillum molischianum. *Journal Of Structural Biology* 152:221-228.

19. Greenwood,J., G.Pryce, L.Devin, W.L.dos-Santos, V.L.Calder, and P.Adamson. 1996. SV40 large T immortalised cell lines of the rat blood-brain and blood-retinal barriers retain their phenotypic and immunological characteristics. *Journal of Neuroimmunology* 71:51-63.

20. Han,D., W.Y.Ma, F.L.Liao, and D.Y.Chen. 2004. Intracellular structural changes under the stress of applied force at a nanometre range investigated by atomic force microscopy. *Nanotechnology* 15:120-126.

21. Hansma,H.G., K.A.Browne, M.Bezanilla, and T.C.Bruice. 1994. Bending and Straightening of Dna Induced by the Same Ligand - Characterization with the Atomic-Force Microscope. *Biochemistry* 33:8436-8441.

22. Hansma,H.G. and J.H.Hoh. 1994. Biomolecular imaging with atomic-force microscope. *Annual Review Of Biophysics And Biomolecular Structure* 23:115-139.

23. Hansma,H.G., R.L.Sinsheimer, J.Groppe, T.C.Bruice, V.Elings, G.Gurley, M.Bezanilla, I.A.Mastrangelo, P.V.C.Hough, and P.K.Hansma. 1993. Recent Advances in Atomic-Force Microscopy of Dna. *Scanning* 15:296-299.

24. Hansma,H.G., R.L.Sinsheimer, M.Q.Li, and P.K.Hansma. 1992. Atomic Force Microscopy of Single-Stranded and Double-Stranded Dna. *Nucleic Acids Research* 20:3585-3590.

25. Hassan,E.A., W.F.Heinz, M.D.Antonik, N.P.D'Costa, S.Nageswaran, C.A.Schoenenberger, and J.H.Hoh. 1998. Relative microelastic mapping of living cells by atomic force microscopy. *Biophysical Journal* 74:1564-1578.

26. Hawkins,B.T. and T.P.Davis. 2005. The blood-brain barrier/neurovascular unit in health and disease. *Pharmacological Reviews* 57:173-185.

27. Hernadi,K., A.Siska, L.Thien-Nga, L.Forro, and I.Kiricsi. 2001. Reactivity of different kinds of carbon during oxidative purification of catalytically prepared carbon nanotubes. *Solid State Ionics* 141:203-209.

28. Hertz,M.G. 1881. Uber die Beruhrung Fester Elastischer Korper. *J. Reine Angew. Math.* 92:156-171.

29. Hofmann,U.G., C.Rotsch, W.J.Parak, and M.Radmacher. 1997. Investigating the cytoskeleton of chicken cardiocytes with the atomic force microscope. *Journal Of Structural Biology* 119:84-91.

30. Hoh,J.H. and C.A.Schoenenberger. 1994. Surface-Morphology and Mechanical-Properties of Mdck Monolayers by Atomic-Force Microscopy. *Journal Of Cell Science* 107:1105-1114.

31. Hutter,J.L. and J.Bechhoefer. 1993. Calibration of Atomic-Force Microscope Tips. *Review Of Scientific Instruments* 64:1868-1873.

32. Ivanov,A.I., A.Nusrat, and C.A.Parkos. 2004. Endocytosis of epithelial apical junctional proteins by a clathrin-mediated pathway into a unique storage compartment. *Molecular Biology of the Cell* 15:176-188.

33. Jimenez-Garcia,L.F. and R.Fragoso-Soriano. 2000. Atomic force microscopy of the cell nucleus. *Journal Of Structural Biology* 129:218-222.

34. Kalderon,D., W.D.Richardson, A.F.Markham, and A.E.Smith. 1984. Sequence Requirements for Nuclear Location of Simian Virus-40 Large-T-Antigen. *Nature* 311:33-38.

35. Kellermayer,M.S.Z., C.Bustamante, and H.L.Granzier. 2003. Mechanics and structure of titin oligomers explored with atomic force microscopy. *Biochimica Et Biophysica Acta-Bioenergetics* 1604:105-114.

36. Kim,J.M., H.S.Jung, J.W.Park, H.Y.Lee, and T.Kawai. 2004. AFM phase lag mapping for protein-DNA oligonucleotide complexes. *Analytica Chimica Acta* 525:151-157.

37. Kroll,R.A. and E.A.Neuwelt. 1998. Outwitting the blood-brain barrier for therapeutic purposes: osmotic opening and other means. *Neurosurgery* 42:1083-1099.

38. Kuznetsov,Y.G., A.J.Malkin, and A.McPherson. 1997. Atomic force microscopy studies of living cells: Visualization of motility, division, aggregation, transformation, and apoptosis. *Journal Of Structural Biology* 120:180-191.

39. Le Grimellec,C., E.Lesniewska, M.C.Giocondi, E.Finot, V.Vie, and J.P.Goudonnet. 1998. Imaging of the surface of living cells by low-force contact- mode atomic force microscopy. *Biophysical Journal* 75:695-703.

40. Luo,D. and W.M.Saltzman. 2000. Synthetic DNA delivery systems. *Nature Biotechnology* 18:33-37.

41. Mahaffy,R.E., S.Park, E.Gerde, J.Kas, and C.K.Shih. 2004. Quantitative analysis of the viscoelastic properties of thin regions of fibroblasts using atomic force microscopy. *Biophysical Journal* 86:1777-1793.

42. Mathur,A.B., A.M.Collinsworth, W.M.Reichert, W.E.Kraus, and G.A.Truskey. 2001. Endothelial, cardiac muscle and skeletal muscle exhibit different viscous and elastic properties as determined by atomic force microscopy. *Journal of Biomechanics* 34:1545-1553.

43. Mourougou-Candoni,N., C.Naud, and F.Thibaudau. 2003. Adsorption of thiolated oligonucleotides on gold surfaces: An atomic force microscopy study. *Langmuir* 19:682-686.

44. Muller,D.J., H.J.Sass, S.A.Muller, G.Buldt, and H.A.Engel. 1999. Surface structures of native bacteriorhodopsin depend on the molecular packing arrangement in the membrane. *Journal Of Molecular Biology* 285:1903-1909.

45. Muller,D.J., F.A.Schabert, G.Buldt, and H.A.Engel. 1995. ImagingPurple membrane in aqueous-solutions at subnanometer resolution by atomic-force microscopy. *Biophysical Journal* 68:1681-1686.

46. Muller,D.J., C.A.Schoenenberger, F.A.Schabert, and H.A.Engel. 1997. Structural changes in native membrane proteins monitored at subnanometer resolution with the atomic force microscope: A review. *Journal Of Structural Biology* 119:149-157.

47. Neuwelt,E.A., D.L.Goldman, S.A.Dahlborg, J.Crossen, F.Ramsey, S.Roman-Goldstein, R.Brazile, and B.Dana. 1991. Primary CNS lymphoma treated with osmotic blood-brain barrier disruption: prolonged survival and preservation of cognitive function. *Journal of Clinical Oncology* 9:1580-1590.

48. Oberleithner,H., S.W.Schneider, L.Albermann, U.Hillebrand, T.Ludwig, C.Riethmuller, V.Shahin, C.Schafer, and H.Schillers. 2003. Endothelial cell swelling by aldosterone. *Journal of Membrane Biology* 196:163-172.

49. Okamura,M.Y., M.L.Paddock, M.S.Graige, and G.Feher. 2000. Proton and electron transfer in bacterial reaction centers. *Biochimica Et Biophysica Acta-Bioenergetics* 1458:148-163.

50. Pardridge,W.M. 2002. Drug and gene delivery to brain: the vascular rout. *Neuron* 36:555-558.

51. Pesen,D. and J.H.Hoh. 2005a. Micromechanical architecture of the endothelial cell cortex. *Biophysical Journal* 88:670-679.

52. Pesen,D. and J.H.Hoh. 2005b. Modes of remodeling in the cortical cytoskeleton of vascular endothelial cells. *Febs Letters* 579:473-476.

53. Pfister,G., C.M.Stroh, H.Perschinka, M.Kind, M.Knoflach, P.Hinterdorfer, and G.Wick. 2005. Detection of HSP60 on the membrane surface of stressed human endothelial cells by atomic force and confocal microscopy. *Journal Of Cell Science* 118:1587-1594.

54. Quist,A.P., S.K.Rhee, H.Lin, and R.Lal. 2000. Physiological role of gap-junctional hemichannels: Extracellular calcium-dependent isosmotic volume regulation. *Journal of Cell Biology* 148:1063-1074.

55. Radmacher,M., M.Fritz, C.M.Kacher, J.P.Cleveland, and P.K.Hansma. 1996. Measuring the viscoelastic properties of human platlets with the atomic force microscope. *Biophysical Journal* 70:556-567.

56. Rappoport,S.I., W.R.Fredeicks, K.Ohno, and K.D.Pettigrew. 2000. Quantitative aspects of reversible osmotic opening of blood-brain barrier. *American Journal Of Physiology* 238:R421-431.

57. Rotsch,C. and M.Radmacher. 2000. Drug-induced changes of cytoskeletal structure and mechanics in fibroblasts: An atomic force microscopy study. *Biophysical Journal* 78:520-535.

58. Rousso,I., E.Khachatryan, I.Brodsky, R.Nachustai, M.Ottolenghi, M.Sheves, and A.Lewis. 1997. Atomic force sensing of light-induced protein dynamics with microsecond time resolution in bacteriorhodopsin and photosynthetic reaction centers. *Journal Of Structural Biology* 119:158-164.

59. Sato,H., N.Kataoka, F.Kajiya, M.Katano, T.Takigawa, and T.Masuda. 2004. Kinetic study on the elastic change of vascular endothelial cells on collagen matrices by atomic force microscopy. *Colloids And Surfaces B-Biointerfaces* 34:141-146.

60. Scheuring,S., D.Levy, and J.L.Rigaud. 2005. Watching the components of photosynthetic bacterial membranes and their in situ organisation by atomic force microscopy. *Biochimica et Biophysica Acta-Biomembranes* 1712:109-127.

61. Scheuring,S., J.N.Sturgis, V.Prima, A.Bernadac, D.Levy, and J.L.Rigaud. 2004. Watching the photosynthetic apparatus in native membranes. *Proceedings Of The National Academy Of Sciences Of The United States Of America* 101:11293-11297.

62. Sharma,A., K.Anderson, and D.J.Muller. 2005. Actin microridges characterized by laser scanning confocal and atomic force microscopy. *Febs Letters* 579:2001-2008.

63. Sneddon,I.N. 1965. The relation between load and penetration in the axisymmetric Boussinesq problem for a punch of arbitrary profile. *Int. J. Engr. Sci.* 3:47-57.

64. Stewart,J.M. and J.D.Young. 1984. Solid Phase Peptide Synthesis. *Pierce Chemical Company, Rockford, IL.*

65. Tandori,J., L.Nagy, A.Puskas, M.Droppa, G.Horvath, and P.Maroti. 1995. The Ile(L229)-]Met Mutation Impairs the Quinone Binding to the Q(B)-Pocket in Reaction Centers of Rhodobacter-Sphaeroides. *Photosynthesis Research* 45:135-146.

66. Vinckier,A. and G.Semenza. 1998. Measuring elasticity of biological materials by atomic force microscopy. *Febs Letters* 430:12-16.

67. Wojcikiewicz,E.P., X.Zhang, and V.T.Moy. 2004. Force and compliance measurements on living cells using atomic force microscopy (AFM). *Biological Procedures Online* 6:1-9.

68. Wu,H.W., T.Kuhn, and V.T.Moy. 1998. Mechanical properties of l929 cells measured by atomic force microscopy: Effects of anticytoskeletal drugs and membrane crosslinking. *Scanning* 20:389-397.

69. Zhang,X., A.Chen, D.De Leon, H.Li, E.Noiri, V.T.Moy, and M.S.Goligorsky. 2003. Atomic force microscopy measurement of leukocyte-endothelial interaction. *American Journal Of Physiology Hart and Circulatory Physiology* 286:H359-367.

Annex